Editors' Suggestion

Evaluation of the three-flavor quark-disconnected contribution to the muon anomalous magnetic moment from experimental data

Diogo Boito,[1,2] Maarten Golterman,[3,4] Kim Maltman,[5,6] and Santiago Peris[4]

[1]*Instituto de Física de São Carlos, Universidade de São Paulo, CP 369, 13570-970 São Carlos, São Paulo, Brazil*
[2]*University of Vienna, Faculty of Physics, Boltzmanngasse 5, A-1090 Wien, Austria*
[3]*Department of Physics and Astronomy, San Francisco State University, San Francisco, California 94132, USA*
[4]*Department of Physics and IFAE-BIST, Universitat Autònoma de Barcelona, E-08193 Bellaterra, Barcelona, Spain*
[5]*Department of Mathematics and Statistics, York University, Toronto, Ontario M3J 1P3, Canada*
[6]*CSSM, University of Adelaide, Adelaide, South Australia 5005, Australia*

(Received 22 March 2022; accepted 22 April 2022; published 16 May 2022)

We point out that the sum of the strange-quark-connected and full three-flavor quark-disconnected contributions to the leading-order hadronic vacuum polarization contribution, $a_\mu^{\mathrm{LO,HVP}}$, to the anomalous magnetic moment of the muon is a physical observable, and we provide a data-based determination of this quantity in the isospin limit. The result, $40.1(1.5) \times 10^{-10}$ or $38.7(2.0) \times 10^{-10}$, depending on which data compilation is used, serves as a target of comparison for lattice calculations of the same isospin-limit combination. Subtracting from this result the average of lattice determinations of the strange-quark-connected contribution, one also obtains an alternate determination of the isospin-limit three-flavor disconnected contribution to $a_\mu^{\mathrm{LO,HVP}}$. The result of this determination, $-13.3(1.5) \times 10^{-10}$ or $-14.6(2.0) \times 10^{-10}$, depending on which data compilation is used, agrees well and is competitive with the most precise current lattice determination.

DOI: 10.1103/PhysRevD.105.093003

I. INTRODUCTION

Interest in reducing the uncertainty on the Standard Model (SM) prediction for a_μ, the anomalous magnetic moment of the muon, increased dramatically with the release of the 2006 BNL E821 experimental result [1], which showed a more than 3.5σ tension with then-existing SM expectations. This interest was further heightened with the release of the first results from the Fermilab E989 experiment [2], which raised the discrepancy between the SM expectation and the experimental world average to the 4.2σ level. The main source of uncertainty in the SM prediction is currently that on hadronic contributions, in particular, the leading-order (LO) hadronic vacuum polarization (HVP) contribution, $a_\mu^{\mathrm{LO,HVP}}$. While a dispersive evaluation of this contribution is possible using experimental hadronic cross-section data, the result in fact represents the SM expectation for this quantity only if beyond-the-SM contributions to the appropriately weighted integral of the experimental cross sections are numerically negligible. While this is likely the case at the current level of precision, a first-principles lattice determination of the SM expectation for $a_\mu^{\mathrm{LO,HVP}}$ is of interest in its own right, and there has been intense recent activity aimed at reducing the uncertainty on such lattice determinations [3–24], with the most recent BMW Collaboration result [20] reaching, for the first time in a lattice determination, the subpercent precision level. First-principles lattice determinations also avoid experimental issues present in the alternate dispersive determination, such as the impact of the long-standing inconsistencies between the *BABAR* and KLOE results for the $e^+e^- \to \pi^+\pi^-$ cross sections.

Lattice determinations of $a_\mu^{\mathrm{LO,HVP}}$ typically involve evaluating and summing isospin-limit light-, strange-, charm-, and bottom-quark-connected contributions, the isospin-limit-disconnected contribution, and both electromagnetic (EM) and strong isospin-breaking (SIB) contributions.[1] The lattice calculation of the disconnected

[1]By "isospin limit," we will always mean pure QCD with no EM corrections and $m_d = m_u$.

contribution is particularly numerically intensive, and only a limited number of lattice results exist for this quantity.

Comparisons between the results from different lattice collaborations for each of the individual flavor-specific-connected contributions, the disconnected contribution, and the EM and SIB contributions are useful for identifying and controlling lattice systematic effects, as are comparisons between results from different groups for related quantities such as the intermediate-Euclidean-time-window integrals, a_μ^W, introduced by RBC/UKQCD [11]. The window quantities are also of interest since they have alternate dispersive representations and hence allow comparisons of data-based lattice and dispersive results for contributions to $a_\mu^{\rm LO,HVP}$ from different windows in Euclidean time. Additional observables amenable to both lattice and dispersive determinations, ideally with relative $I = 1$ and $I = 0$ contributions that differ from those of the RBC/UKQCD window quantities, would be of interest for a similar reason.

In this paper, we point out that the sum of strange-quark-connected and full three-flavor-disconnected contributions to $a_\mu^{\rm LO,HVP}$, denoted as $a_\mu^{\rm sconn+disc}$ in what follows, provides an example of such an additional observable, one with a significantly higher relative weight for $I = 0$ contributions. We then show how existing experimental results can be used to obtain a data-based determination of $a_\mu^{\rm sconn+disc}$. The precision on this determination turns out to be such that, using existing lattice results for the strange-quark-connected contribution, one is able to determine the three-flavor disconnected contribution to $a_\mu^{\rm LO,HVP}$ with a precision comparable to that of the best current lattice determination.

The rest of the paper is organized as follows. Section II lays out some relevant background and notation, while Sec. III outlines the basic analysis approach. Section IV provides details of a numerical implementation using as input (i) the results of the *BABAR* determination of the differential $\tau \to K^- K^0 \nu_\tau$ decay distribution [25] and (ii) the assessment of exclusive-mode $e^+e^- \to$ hadrons cross sections and exclusive-mode contributions to $a_\mu^{\rm LO,HVP}$ detailed in Refs. [26,27]. In Sec. V, we discuss isospin-breaking corrections to the results obtained in Sec. IV that are needed to make contact with isospin-symmetric lattice results. Section VI outlines an alternate version of the full analysis employing, in place of the exclusive-mode $a_\mu^{\rm LO,HVP}$ contributions of Refs. [26,27], the alternate set of such contributions from Ref. [28]. Finally, in Sec. VII, we summarize and briefly discuss our results. In the rest of the paper we will, for the sake of brevity, use the shorter forms "disconnected contribution" and "strange-quark-connected plus disconnected contribution" in place of the more accurate, but longer, expressions "full three-flavor disconnected contribution" and "strange-quark-connected plus full three-flavor disconnected contribution."

II. NOTATION AND BACKGROUND

In this section, we define our notation and introduce a number of useful decompositions. We denote the flavor octet of light- and strange-quark vector currents as $V_\mu^a = \bar q \frac{\lambda^a}{2} \gamma_\mu q$, $a = 1, \ldots, 8$, with q the column vector $(u, d, s)^T$. This allows us to define the vector-current two-point functions, $\Pi_{\mu\nu}^{ab}(q)$, their associated polarizations, $\Pi^{ab}(Q^2)$, and the associated spectral functions, $\rho^{ab}(s)$, with $s = q^2$ and $Q^2 = -q^2$, as usual, by

$$\begin{aligned}\Pi_{\mu\nu}^{ab}(q) &= (q_\mu q_\nu - q^2 g_{\mu\nu})\Pi^{ab}(Q^2) \\ &= i \int d^4x e^{iq\cdot x} \langle 0|T(V_\mu^a(x) V_\nu^b(0))|0\rangle, \end{aligned} \tag{2.1}$$

$$\rho^{ab}(s) = \frac{1}{\pi} {\rm Im}\Pi^{ab}(Q^2), \qquad (s = -Q^2 > 0), \tag{2.2}$$

and the subtracted polarizations, $\hat\Pi^{ab}(Q^2)$, by

$$\hat\Pi^{ab}(Q^2) = \Pi^{ab}(Q^2) - \Pi^{ab}(0). \tag{2.3}$$

The $(u,\ d,\ s)$ part of the EM current, $J_\mu^{\rm EM}$, has the decomposition

$$\begin{aligned} J_\mu^{\rm EM} &= V_\mu^3 + \frac{1}{\sqrt{3}} V_\mu^8 \equiv J_\mu^{\rm EM,3} + J_\mu^{\rm EM,8} \\ &= \frac{1}{2}(\bar u \gamma_\mu u - \bar d \gamma_\mu d) + \frac{1}{6}(\bar u \gamma_\mu u + \bar d \gamma_\mu d - 2\bar s \gamma_\mu s) \end{aligned} \tag{2.4}$$

into $I = 1$ $(a = 3)$ and $I = 0$ $(a = 8)$ parts. We also define, for use below, the coefficients c_k^a, $k = u,\ d,\ s$ and $a = 3,\ 8$ via

$$J_\mu^{{\rm EM},a} \equiv \sum_{k=u,d,s} c_k^a \bar q \gamma_\mu q. \tag{2.5}$$

The values are $c_u^3 = -c_d^3 = 1/2$, $c_s^3 = 0$ and $c_u^8 = c_d^8 = 1/6$, $c_s^8 = -2/6$.

The subtracted three-flavor EM vacuum polarization and the associated spectral function, $\rho_{\rm EM}(s)$, have related decompositions,

$$\begin{aligned} \hat\Pi_{\rm EM}(Q^2) &= \hat\Pi_{\rm EM}^{33}(Q^2) + \frac{2}{\sqrt{3}} \hat\Pi_{\rm EM}^{38}(Q^2) + \frac{1}{3} \hat\Pi_{\rm EM}^{88}(Q^2) \\ &\equiv \hat\Pi_{\rm EM}^{I=1}(Q^2) + \hat\Pi_{\rm EM}^{\rm MI}(Q^2) + \hat\Pi_{\rm EM}^{I=0}(Q^2), \\ \rho_{\rm EM}(s) &= \rho^{33}(s) + \frac{2}{\sqrt{3}} \rho^{38}(s) + \frac{1}{3} \rho^{88}(s) \\ &\equiv \rho_{\rm EM}^{I=1}(s) + \rho_{\rm EM}^{\rm MI}(s) + \rho_{\rm EM}^{I=0}(s), \end{aligned} \tag{2.6}$$

into pure isovector $(ab = 33,\ I = 1)$, pure isoscalar $(ab = 88,\ I = 0)$, and mixed-isospin (MI) $(ab = 38,\ 83)$ parts, with the latter, of course, vanishing in the isospin limit. In the isospin limit, $\hat\Pi^{33}$ has only light-quark-connected contributions, while $\hat\Pi^{88}$ is a sum of light-quark-connected, strange-quark-connected, and all disconnected contributions.

The hadronic contribution $a_\mu^{\rm LO,HVP}$ can be determined using the standard "dispersive" representation

$$a_\mu^{\rm LO,HVP} = \frac{\alpha_{\rm EM}^2 m_\mu^2}{9\pi^2}\int_{m_\pi^2}^{\infty} ds\,\frac{\hat{K}(s)}{s^2}R(s), \tag{2.7}$$

where $\alpha_{\rm EM}$ is the EM fine-structure constant, $R(s)$ is the standard EM cross-section ratio,

$$R(s) = \frac{3s}{4\pi\alpha_{\rm EM}^2}\sigma^{(0)}[e^+e^- \to \text{hadrons}(+\gamma)], \tag{2.8}$$

with $\sigma^{(0)}[e^+e^- \to \text{hadrons}(+\gamma)]$ the bare inclusive hadronic electroproduction cross section. The kernel $\hat{K}(s)$ is exactly known and slowly (and monotonically) increasing with s (see, for example, Ref. [29]). The dispersive determination typically employs a sum of exclusive-mode contributions up to just below $s = 4\ \text{GeV}^2$, and inclusive $R(s)$ determinations and/or perturbative QCD (pQCD) above that, apart from in the region of narrow charm and bottom resonances. Using the decomposition of Eq. (2.6) for the EM spectral function, and the relation

$$R(s) = 12\pi^2\rho_{\rm EM}(s), \tag{2.9}$$

the three-flavor contribution to $a_\mu^{\rm LO,HVP}$ can also be broken down into $I = 1$ (33), $I = 0$ (88), and mixed-isospin (MI, $38 + 83$) contributions,

$$a_\mu^{\rm LO,HVP} = a_\mu^{33} + \frac{2}{\sqrt{3}}a_\mu^{38} + \frac{1}{3}a_\mu^{88} \equiv a_\mu^{I=1} + a_\mu^{\rm MI} + a_\mu^{I=0}. \tag{2.10}$$

Contributions to these quantities from an individual exclusive mode, X, can also be defined, and are denoted as $[a_\mu^{\rm LO,HVP}]_X$, $[a_\mu^{I=1}]_X$, $[a_\mu^{I=0}]_X$, and $[a_\mu^{\rm MI}]_X$.

The hadronic contribution $a_\mu^{\rm LO,HVP}$ also has the standard weighted Euclidean-Q^2 integral representation [30–32],

$$a_\mu^{\rm LO,HVP} = -4\alpha_{\rm EM}^2\int_0^\infty dQ^2 f(Q^2)\hat{\Pi}_{\rm EM}(Q^2), \tag{2.11}$$

with $f(Q^2)$ another exactly known kernel which diverges as $1/\sqrt{Q^2}$ as $Q^2 \to 0$, and creates a peak in the integrand of Eq. (2.11) at very low $Q^2 \simeq m_\mu^2/4$. This expression, or the related time-momentum representation [33], forms the basis for lattice determinations of $a_\mu^{\rm LO,HVP}$. Analogous representations for $a_\mu^{I=1}$, $a_\mu^{I=0}$, and $a_\mu^{\rm MI}$ are obtained by replacing $\hat{\Pi}_{\rm EM}$ in Eq. (2.11) with $\hat{\Pi}_{\rm EM}^{I=1}$, $\hat{\Pi}_{\rm EM}^{I=0}$, and $\hat{\Pi}_{\rm EM}^{\rm MI}$, respectively. To first order in $m_d - m_u$, there are no SIB contributions to either a_μ^{33} or a_μ^{88}, while SIB is expected to dominate a_μ^{38}.

III. THE BASIC IDEA

The basic idea of the analysis is the following. In the isospin limit, $\hat{\Pi}_{\rm EM}^{I=1}$ receives only light-quark-connected contributions, while $\hat{\Pi}_{\rm EM}^{I=0}$ is a sum of light-quark-connected, strange-quark-connected, and all disconnected contributions. It is thus obvious that there is a combination of $\hat{\Pi}_{\rm EM}^{I=1}$ and $\hat{\Pi}_{\rm EM}^{I=0}$ in which the light-quark-connected contributions cancel, leaving a result which is the sum of the strange-quark-connected and disconnected contributions. It is easy to check (as noted explicitly in Ref. [4]) that this combination is

$$\hat{\Pi}_{\rm EM}^{\rm sconn+disc} \equiv \hat{\Pi}_{\rm EM}^{I=0} - \frac{1}{9}\hat{\Pi}_{\rm EM}^{I=1}. \tag{3.1}$$

The corresponding spectral function is

$$\rho_{\rm EM}^{\rm sconn+disc}(s) = \rho_{\rm EM}^{I=0}(s) - \frac{1}{9}\rho_{\rm EM}^{I=1}(s). \tag{3.2}$$

The appropriately weighted dispersive integral of the latter combination produces a result, $a_\mu^{\rm sconn+disc}$, which is the sum of the strange-quark-connected and disconnected contributions to $a_\mu^{\rm LO,HVP}$. It follows that, if the $I = 0$ and $I = 1$ contributions to $R(s)$ can be separated with sufficient precision, an accurate experimental determination of this combination will be possible. In terms of the $I = 0$ and $I = 1$ contributions to $a_\mu^{\rm LO,HVP}$,

$$a_\mu^{\rm sconn+disc} = a_\mu^{I=0} - \frac{1}{9}a_\mu^{I=1}. \tag{3.3}$$

Such a determination would serve as a useful target of comparison for lattice determinations of the same sum.

The strange-quark-connected contribution to $a_\mu^{\rm LO,HVP}$, $a_\mu^{\rm sconn}$, has been rather precisely determined by several lattice groups [3,6,9,11,12,16,18,20]. The most recent (BMW) determination, $53.393(89)(68) \times 10^{-10}$ [20], is in excellent agreement with the average, $(53.2 \pm 0.3) \times 10^{-10}$, of previous determinations quoted in the 2020 $g-2$ Theory Initiative white paper [29]. $a_\mu^{\rm sconn}$ is thus already known to much higher precision than the final target $\sim 1.4 \times 10^{-10}$ uncertainty on a_μ expected from the full FNAL E989 experimental program. In view of this precision, an experimental determination of $a_\mu^{\rm sconn+disc}$ will also provide a determination, with comparable precision, of the full disconnected contribution to $a_\mu^{\rm LO,HVP}$, $a_\mu^{\rm disc} = a_\mu^{\rm sconn+disc} - a_\mu^{\rm sconn}$. All this, of course, assumes the experimentally determined $a_\mu^{\rm sconn+disc}$ combination does not contain significant beyond-the-SM contributions and hence should be compatible with SM-based lattice determinations of this quantity.

In Sec. IV, we will implement this idea neglecting, to begin with, isospin-breaking (IB) corrections. Then, in

Sec. V, we will take into account IB corrections to arrive at our final results for $a_\mu^{\rm sconn+disc}$ and $a_\mu^{\rm disc}$.

IV. AN IMPLEMENTATION WITH CURRENT EXPERIMENTAL DATA

In what follows, we employ the dispersive results for exclusive-mode contributions to $a_\mu^{\rm LO,HVP}$ from the region $\sqrt{s} \leq 1.937$ GeV, listed in Table 1 of Ref. [27] (which we will refer to as KNT2019). Above $s = 1.937^2$ GeV^2, we use the five-loop, $n_f = 3$ pQCD expression for $\rho_{\rm EM}^{\rm sconn+disc}(s)$, with PDG2020 input for α_s [34]. It is straightforward to show that the pQCD result for $\rho_{\rm EM}^{\rm sconn+disc}(s)$ is one-sixth that of the $\rho_{\rm EM}(s)$ result, in the chiral limit, with small corrections proportional to m_s^2/s. The approximation of using the pQCD representation for $\rho_{\rm EM}^{\rm sconn+disc}(s)$ in this region is expected to be an accurate one, up to possible small duality-violating corrections. As illustrated in Fig. 12 of Ref. [29], $n_f = 3$ pQCD expectations for $R(s)$ agree within errors with experimental determinations [35–37] (especially those of KEDR [37]) in the region from slightly below $\sqrt{s} = 2$ GeV up to the charm threshold.

The main part of the $I = 1/I = 0$ separation of exclusive-mode contributions is accomplished, as usual, using G parity. Exclusive modes with positive (negative) G parity have $I = 1$ ($I = 0$). This allows unique isospin assignments for contributions from exclusive modes consisting entirely of strong-interaction-stable and/or narrow states with well-defined G parity (π, η, ω, ϕ). Such modes account for more than 93% of the contribution to $a_\mu^{\rm LO,HVP}$ from the KNT2019 exclusive-mode region.

Additional information is required to separate the $I = 1$ and $I = 0$ components of the contributions of exclusive modes containing at least one $K\bar{K}$ pair, which are not eigenstates of G parity. We discuss below how this separation can be accomplished using experimental input in the case of the $K\bar{K}$ and $K\bar{K}\pi$ exclusive modes. For all remaining KNT2019 G-parity-ambiguous exclusive modes, X, whose spectral contributions lie at higher s and whose contributions to $a_\mu^{\rm LO,HVP}$ are thus strongly numerically suppressed, we use a "maximally conservative" assessment of the desired $[a_\mu^{\rm sconn+disc}]_X = [a_\mu^{I=0}]_X - \frac{1}{9}[a_\mu^{I=1}]_X$ combination, determined as follows. Since the $I = 0$ contribution for mode X can, in principle, lie anywhere between 0 and the full mode-X $I = 0 + 1$ total, $[a_\mu^{\rm LO,HVP}]_X$, the $[a_\mu^{\rm sconn+disc}]_X$ combination we are interested in necessarily lies between $-\frac{1}{9}[a_\mu^{\rm LO,HVP}]_X$ and $[a_\mu^{\rm LO,HVP}]_X$.[2] One may thus be maximally conservative and cover this entire range by taking

$$[a_\mu^{\rm sconn+disc}]_X = \left(\frac{4}{9} \pm \frac{5}{9}\right)[a_\mu^{\rm LO,HVP}]_X. \tag{4.1}$$

We now turn to the explicit numerical determination of the strange-quark-connected plus full disconnected sum, using the data input and analysis strategies outlined above and described in more detail below. Note that the KNT2019 results used below for all G-parity-unambiguous exclusive-mode contributions are the contributions of these modes between the threshold and $\sqrt{s} = 1.937$ GeV. Inclusive input is used above this point. In what follows, we outline how additional experimental input can be used to fix the $I = 1$ contributions, $[\rho_{\rm EM}^{I=1}(s)]_X$, to $\rho_{\rm EM}(s)$, and hence also the $I = 1$ contributions $[a_\mu^{I=1}]_X$ for the exclusive modes $X = K\bar{K}$ and $K\bar{K}\pi$. By carrying out the $[\rho_{\rm EM}^{I=1}(s)]_X$ determinations over the full KNT2019 exclusive-mode region, $\sqrt{s} \leq 1.937$ GeV, the associated $I = 0$ contributions, and hence also the desired $[a_\mu^{\rm sconn+disc}]_X$ combinations, for that same region follow immediately from the corresponding KNT2019 total $I = 0 + 1$ $[a_\mu^{\rm LO,HVP}]_X$ results.

A. G-parity-unambiguous modes

The results of Table I of KNT2019 for the G-parity-unambiguous exclusive-mode contributions to $a_\mu^{\rm LO,HVP}$ from the region between the threshold and $\sqrt{s} = 1.937$ GeV are tabulated in Table I. From this table, the contribution of all G-parity-unambiguous exclusive modes to the sum of the strange-quark-connected and disconnected contributions to $a_\mu^{\rm LO,HVP}$ is

$$\left[55.10(96) - \frac{543.21(2.09)}{9}\right] \times 10^{-10} = -5.26(99) \times 10^{-10}. \tag{4.2}$$

B. $K\bar{K}$ modes

The sum of the two $K\bar{K}$-mode contributions to $a_\mu^{\rm LO,HVP}$ in KNT2019, $(23.03(22) + 13.04(19)) \times 10^{-10}$, is sufficiently large that the error produced by the maximally conservative $I = 0/1$ separation assessment would be far too large to make the resulting determination of the disconnected contribution useful. The $K\bar{K}$ contributions are, however, expected to be dominated by those of the $I = 0$ ϕ resonance, and the measured cross sections for both charge modes do, in keeping with this expectation, show very large peaks in the ϕ region. We need to turn this qualitative expectation into something more quantitative. This can be done using the conserved vector current relation and recent *BABAR* results for the unit-normalized differential $\tau \to K\bar{K}\nu_\tau$ decay distribution [25]. The latter, normalized to reproduce the corresponding branching fraction, gives an experimental determination of the charged $I = 1$, vector-current spectral function [38] [the

[2]Explicitly: if x is the fraction of the total that is $I = 0$, the $I = 1$ fraction is $1 - x$, and the $(I = 0) - (1/9)(I = 1)$ combination a fraction $x - (1/9)(1 - x) = (10/9)x - (1/9)$ of the total. This result is monotonic in x, increasing from $-1/9$ at $x = 0$ to 1 at $x = 1$.

TABLE I. G-parity-unambiguous exclusive-mode contributions to $a_\mu^{\rm LO,HVP}$ for $\sqrt{s} \le 1.937$ GeV from KNT2019. Entries are in units of 10^{-10}. The notation "npp" is KNT2019's shorthand for "non purely pionic".

$I=1$ modes X	$[a_\mu^{\rm LO,HVP}]_X \times 10^{10}$	$I=0$ modes X	$[a_\mu^{\rm LO,HVP}]_X \times 10^{10}$
Low-s $\pi^+\pi^-$	0.87(02)	Low-s 3π	0.01(00)
$\pi^+\pi^-$	503.46(1.91)	$\pi^0\gamma$ (ω, ϕ dominated)	4.46(10)
$2\pi^+2\pi^-$	14.87(20)	3π	46.73(94)
$\pi^+\pi^-2\pi^0$	19.39(78)	$2\pi^+2\pi^-\pi^0$ (no ω, η)	0.98(09)
$3\pi^+3\pi^-$ (no ω)	0.23(01)	$\pi^+\pi^-3\pi^0$ (no η)	0.62(11)
$2\pi^+2\pi^-2\pi^0$ (no η)	1.35(17)	$3\pi^+3\pi^-\pi^0$ (no ω, η)	0.00(01)
$\pi^+\pi^-4\pi^0$ (no η)	0.21(21)	$\eta\gamma$ (ω, ϕ dominated)	0.70(02)
$\eta\pi^+\pi^-$	1.34(05)	$\eta\pi^+\pi^-\pi^0$ (no ω)	0.71(08)
$\eta 2\pi^+2\pi^-$	0.08(01)	$\eta\omega$	0.30(02)
$\eta\pi^+\pi^-2\pi^0$	0.12(02)	$\omega(\to npp)2\pi$	0.13(01)
$\omega(\to \pi^0\gamma)\pi^0$	0.88(02)	$\omega 2\pi^+2\pi^-$	0.01(00)
$\omega(\to npp)3\pi$	0.17(03)	$\eta\phi$	0.41(02)
$\omega\eta\pi^0$	0.24(05)	$\phi \to$ unaccounted	0.04(04)
Total:	543.21(2.09)	Total:	55.10(96)

isospin partner of $\rho^{I=1}_{\rm EM}(s)$], and hence provides a determination of the $I=1$ $e^+e^- \to K\bar{K}$ contribution to $R(s)$ in the region $s < m_\tau^2$ that is kinematically accessible in τ decay.[3] We have used the *BABAR* results to carry out this determination up to $s = 2.7556\ \text{GeV}^2$ (which corresponds to using all but the last *BABAR* bin, which is not used, because of its large width and gigantic statistical error). This produces a contribution of $0.764(9)(26)(18) \times 10^{-10}$ to $[a_\mu^{I=1}]_{K\bar{K}}$ from the region $s \le 2.7556\ \text{GeV}^2$, where the first error is statistical, the second is systematic, and the third is that induced by the uncertainty on the $\tau \to K^-K^0\nu_\tau$ branching fraction (taken from the HFLAV 2019 compilation [39]), which sets the overall normalization of the τ-decay distribution. Above this point, we switch back to using $e^+e^- \to K\bar{K}$ cross-section data.[4] Integrating the KNT2019 2-mode, $I=0+1$ $e^+e^- \to K\bar{K}$ cross-section sum from $s = 2.7556\ \text{GeV}^2$ to $(1.937\ \text{GeV})^2 = 3.7520\ \text{GeV}^2$, we find a maximally conservative error assessment of $0.089(89) \times 10^{-10}$ for the $I=1$ contribution from this region.[5] Combining this result with that from the region below $s = 2.7556\ \text{GeV}^2$, we find a total $I=1$ $K\bar{K}$ contribution to $a_\mu^{\rm LO,HVP}$ from the region $s \le (1.937\ \text{GeV})^2 = 3.7520\ \text{GeV}^2$ of

$$[a_\mu^{I=1}]_{K\bar{K}} = 0.852(94) \times 10^{-10}. \tag{4.3}$$

The central value in Eq. (4.3) is dominated by the contribution from the region up to $2.7556\ \text{GeV}^2$ determined by the *BABAR* τ-decay data.

With KNT2019 giving a $\sqrt{s} \le 1.937$ GeV $I=0+1$, two-mode $K\bar{K}$ total of

$$\begin{aligned}[a_\mu^{\rm LO,HVP}]_{K\bar{K}} &= (23.03(22) + 13.04(19)) \times 10^{-10} \\ &= 36.07(29) \times 10^{-10},\end{aligned} \tag{4.4}$$

we find an $I=0$ contribution of $35.22(30) \times 10^{-10}$, and hence a $K\bar{K}$ strange-quark-connected plus disconnected contribution from the region up to $\sqrt{s} = 1.937$ GeV of

$$\begin{aligned}[a_\mu^{\rm sconn+disc}]_{K\bar{K}} &\equiv [a_\mu^{I=0}]_{K\bar{K}} - \frac{1}{9}[a_\mu^{I=1}]_{K\bar{K}} \\ &= [a_\mu^{\rm LO,HVP}]_{K\bar{K}} - \frac{10}{9}[a_\mu^{I=1}]_{K\bar{K}} \\ &= 35.12(31) \times 10^{-10}.\end{aligned} \tag{4.5}$$

The error on this result, 0.31×10^{-10}, is dramatically reduced compared to the $\sim 20 \times 10^{-10}$ uncertainty that would result were the *BABAR* τ-decay distribution results not available and one were forced to rely on the maximally conservative assessment.

[3] This is up to (for our purposes) numerically negligible isospin-breaking corrections.

[4] Explicitly, we use the results for the exclusive-mode $e^+e^- \to K^+K^-$ and $e^+e^- \to K_SK_L$ cross sections and covariances employed by KNT2019, which were provided to us by the authors.

[5] Additional constraints, generated using experimental K^+K^- to K_SK_L electroproduction cross-section ratios, in fact, allow this maximally conservative 0.089×10^{-10}, $I=0/1$ separation error to be reduced somewhat, to 0.065×10^{-10}. Since, however, neither the improved nor the larger maximally conservative error is relevant on the scale of the uncertainty in our final results for $a_\mu^{\rm sconn+disc}$ and $a_\mu^{\rm disc}$, we do not discuss this improvement further, and we employ the weaker maximally conservative error assessment in obtaining our final results below.

C. $K\bar{K}\pi$ modes

The separation of the exclusive-mode $K\bar{K}\pi$ cross sections into $I = 0$ and $I = 1$ components was carried out already in 2007 by *BABAR* [40] using a Dalitz plot analysis predicated on the observed saturation of the cross sections by KK^* contributions. This result, combined with conserved vector current, was actually already used, again long ago, by ALEPH to provide a data-based separation of $I = 1$ vector and axial vector contributions to the experimental $\tau \to K\bar{K}\pi\nu_\tau$ distribution [41]. Here we simply convert the *BABAR* $I = 1$ cross-section results to the corresponding $K\bar{K}\pi$ contributions to $R(s)$ and integrate these with the dispersive weight to determine the $I = 1$ part of the $K\bar{K}\pi$ contribution to $a_\mu^{\rm LO,HVP}$. The result is a contribution from the region up to $\sqrt{s} = 1.937$ GeV of

$$[a_\mu^{I=1}]_{K\bar{K}\pi} = 0.741(36)(117) \times 10^{-10} = 0.74(12) \times 10^{-10}, \tag{4.6}$$

where the first error is statistical and the second systematic. With KNT2019 giving an $I = 0 + 1$ total from this same region $[a_\mu^{\rm LO,HVP}]_{K\bar{K}\pi} = 2.71(12) \times 10^{-10}$, we find a strange-quark-connected plus disconnected contribution of

$$\begin{aligned}[a_\mu^{\rm sconn+disc}]_{K\bar{K}\pi} &= [a_\mu^{\rm LO,HVP}]_{K\bar{K}\pi} - \frac{10}{9}[a_\mu^{I=1}]_{K\bar{K}\pi} \\ &= 1.89(18) \times 10^{-10}. \end{aligned} \tag{4.7}$$

For completeness, the corresponding $I = 0$ contribution is $[a_\mu^{I=0}]_{K\bar{K}\pi} = 1.97(17) \times 10^{-10}$.

D. The remaining G-parity-ambiguous modes

The determination of the sum of the strange-quark-connected plus disconnected contributions from all remaining G-parity-ambiguous exclusive modes is detailed in the Appendix. Errors are, in all cases, obtained using the maximally conservative strategy. The result for this sum, $1.05(98) \times 10^{-10}$, has a central value and an uncertainty both dominated by the corresponding $K\bar{K}2\pi$-mode contribution.

E. Perturbative contributions

Finally, we consider the pQCD contribution for the inclusive region [above $s = (1.937\ \text{GeV})^2 = 3.7520\ \text{GeV}^2$]. To set notation, the pQCD expression for the EM-current Adler function, $D(Q^2) = -Q^2 d\Pi_{\rm EM}(Q^2)/Q^2$, is [42]

$$\begin{aligned} D(Q^2) = \frac{1}{6\pi^2}[1 + a(Q^2) + 1.63982a^2(Q^2) + 6.37101a^3(Q^2) \\ + 49.0757a^4(Q^2) + d_5 a^5(Q^2) + \cdots], \end{aligned} \tag{4.8}$$

where $a(Q^2) = \alpha_s(Q^2)/\pi$. The six-loop coefficient, d_5, is not yet known. In what follows, we employ $d_5 = 283$ [43], which is in agreement with recent estimates of this coefficient [44–46]. With this notation, the corresponding pQCD expression for $\rho_{\rm EM}^{\rm sconn+disc}(s)$ is

$$\begin{aligned}[\rho_{\rm EM}^{\rm sconn+disc}(s)]_{\rm pQCD} &= \frac{1}{6}[\rho_{\rm EM}(s)]_{\rm pQCD} \\ &= \frac{1}{36\pi^2}[1 + a(s) + 1.63982a^2(s) \\ &\quad - 10.2839a^3(s) - 106.880a^4(s) \\ &\quad + (d_5 - 779.581)a^5(s) + \cdots]. \end{aligned} \tag{4.9}$$

Integrating this numerically, using as input the $n_f = 3$ result $\alpha_s(m_\tau^2) = 0.3139(71)$, which follows from the 2020 PDG $n_f = 5$ M_Z scale value 0.1179(10), as an example, and, keeping the six-loop term with the Beneke-Jamin $d_5 = 283$ estimate, gives a total inclusive-region $n_f = 3$ contribution to $a_\mu^{\rm sconn+disc}$ of $6.281(5) \times 10^{-10}$. If we turn off all $O(\alpha_s^5)$ contributions, this becomes $6.291(6) \times 10^{-10}$. The quoted uncertainties are those associated with that on the PDG input for α_s and are so small that we ignore them in what follows. The $\sim 0.01 \times 10^{-10}$ difference between the fully known five-loop- and estimated six-loop-truncated results similarly suggests that the uncertainty associated with truncating the pQCD expansion at five loops is negligible on the scale of other errors in our determinations of $a_\mu^{\rm sconn+disc}$ and $a_\mu^{\rm disc}$.

$D = 2$ perturbative corrections in this region will be very small for the following reasons. First, the light-quark-loop contributions to the $I = 0$ and $I = 1$ $D = 2$ perturbative series cancel in the $(I = 0)$-$(1/9)(I = 1)$ combination, and the MI contribution vanishes. This leaves a $D = 2$ expression for the desired strange-quark-connected plus disconnected combination that is entirely that of the strange current $I = 0$ contribution. The resulting $D = 2$ contribution to the desired polarization combination is then easily read off from, for example, the vector-current $D = 2$ expression in Ref. [47] and is (neglecting $m_{u,d}$)

$$\begin{aligned}[\Pi_{\rm EM}^{\rm sconn+disc}(Q^2)]_{D=2} = -\frac{1}{6\pi^2}\frac{m_s^2(Q^2)}{Q^2}\Big[1 + \frac{8}{3}a(Q^2) \\ + 24.1415a^2(Q^2) + \cdots\Big]. \end{aligned} \tag{4.10}$$

From this, it is easily shown that the $D = 2$ contribution to the perturbative representation of $\rho_{\rm EM}^{\rm sconn+disc}(s)$ is

$$[\rho_{\rm EM}^{\rm sconn+disc}(s)]_{D=2} = \frac{1}{6\pi^2}\frac{m_s^2(s)}{s}\Big[2a(s) + \frac{227}{12}a^2(s) + \cdots\Big]. \tag{4.11}$$

The leading term in the $D = 2$ series is thus a factor of $12m_s^2(s)a(s)/s$ times the leading term in the $D = 0$ series. This represents a factor of $\sim 1/400$ suppression of the

leading $D = 2$ relative to the leading $D = 0$ contribution for $s \sim 4$ GeV^2. This rough estimate for the size of the integrated inclusive-region $D = 2$ contribution relative to the corresponding integrated $D = 0$ contribution is borne out by the result of integrating the three-loop-truncated $D = 2$ series, with the integration from $s = (1.937\ \text{GeV})^2$ to infinity producing a $D = 2$ contribution to $a_\mu^{\text{sconn+disc}}$ of 0.012×10^{-10}, to be compared to the result 6.29×10^{-10} for the corresponding five-loop-truncated $D = 0$ contribution.

Still to be carried out is an estimate of the impact of possible small residual exponentially damped quark-hadron duality-violating (DV) contributions to $\rho_{\text{EM}}^{\text{sconn+disc}}(s)$. We also expect these to be small, though not as small as the tiny $D = 2$ corrections. The question of the size of possible DV-induced uncertainties can be explored by updating recent finite-energy-sum-rule (FESR) fits to electroproduction cross-section data and $I = 1$ τ-decay data, in which the parameters of a large-N_c + Regge-motivated ansatz [48] for the s dependence of the DV contribution to the vector $I = 1$ and $I = 0$ spectral functions are obtained as part of the fits. We return to this point in Sec. VII.

Combining the G-parity-unambiguous-mode contributions given in Eq. (4.2) with the $K\bar{K}$ and $K\bar{K}\pi$ contributions given in Eqs. (4.5) and (4.7), the remaining G-parity-ambiguous mode contributions (dominated by $K\bar{K}2\pi$), detailed in the Appendix, and the inclusive region contribution estimated using pQCD, detailed in Sec. IV E, we obtain the following result for the sum of the strange-quark-connected and disconnected contributions to $a_\mu^{\text{LO,HVP}}$:

$$\begin{aligned} a_\mu^{\text{sconn+disc}} &= \left[55.10(96) - \frac{543.21(2.09)}{9} + 35.12(31)\right. \\ &\quad \left. + 1.89(18) + 1.05(98) + 6.28\right] \times 10^{-10} \\ &= 39.08(1.44) \times 10^{-10}. \end{aligned} \tag{4.12}$$

Subtracting from this the $g-2$ Theory Initiative white paper average, $a_\mu^{\text{sconn}} = 53.2(3) \times 10^{-10}$ [29], for the strange-quark-connected contribution, obtained by averaging the results of Refs. [3,6,9,11,12,16,18,20], we find as our initial estimate for the disconnected contribution

$$a_\mu^{\text{disc}} = -14.1(1.5) \times 10^{-10}. \tag{4.13}$$

Expanding the white paper average to include the new BMW result, $a_\mu^{\text{sconn}} = 53.393(89)(68) \times 10^{-10}$ [20], shifts this estimate only slightly, to

$$a_\mu^{\text{disc}} = -14.3(1.4) \times 10^{-10}. \tag{4.14}$$

The disconnected result, Eq. (4.14), is, of course, obtained without having to carry out the numerically intensive determination of disconnected contributions on the lattice. It is, however, not yet directly comparable to current lattice determinations, since the latter are defined in the isospin limit. The exclusive-mode contributions used in obtaining the estimate of Eq. (4.13), in contrast, are physical ones and will include small IB contributions. In the next section, we explore the size of possible IB corrections to the initial estimates for $a_\mu^{\text{sconn+disc}}$ and a_μ^{disc} given in Eqs. (4.12) and (4.14).

V. ESTIMATES FOR ISOSPIN-BREAKING CORRECTIONS

To make contact with the lattice determinations of $a_\mu^{\text{sconn+disc}}$ and a_μ^{disc}, it is necessary to estimate and subtract IB contributions to the results of Eqs. (4.12) and (4.14). We consider strong and EM IB corrections separately. The recent BMW lattice paper [20] is the first to provide determinations of all EM contributions, and, to take advantage of those results in the discussion below, we work with the SIB contribution defined in the same scheme for separating strong and EM IB as used by BMW (defined such that all EM effects in the purely connected neutral pseudoscalar masses are absorbed into the definitions of the quark masses and are numerically very similar to the Gasser-Rusetsky-Scimemi scheme [49]).[6]

To determine the IB corrections to the initial estimates for $a_\mu^{\text{sconn+disc}}$ and a_μ^{disc} obtained above and make contact with isospin-limit lattice results, one needs to identify and subtract the IB contributions present in the experimental versions of the nominal $I = 0$ and $I = 1$ contributions, $a_\mu^{I=0}$ and $a_\mu^{I=1}$, determined above. These are of two types: those belonging to the mixed-isospin (a_μ^{MI}) "contaminations" of the various physical exclusive-mode contributions, and those present in the physical $a_\mu^{I=0}$ and $a_\mu^{I=1}$ contributions themselves. An inclusive determination of the IB contributions present in the physical versions of $a_\mu^{I=0}$ and $a_\mu^{I=1}$ is sufficient to perform the latter correction. Correcting for the mixed-isospin contaminations, however, requires one to identify the mixed-isospin components of the various exclusive-mode $a_\mu^{\text{LO,HVP}}$ contributions.

A rough (likely conservative) estimate for the scale of the IB-induced uncertainty can be obtained by assuming an $O(1\%)$ scale for IB corrections to each of the non pQCD terms in Eq. (4.12) and adding these uncertainties linearly [corresponding to the presumably conservative assumption that all enter the combination in Eq. (4.12) with the same sign]. The result is a first-pass estimate of $\sim 1.5 \times 10^{-10}$ for the IB-induced uncertainty on the result for $a_\mu^{I=0} - \frac{1}{9} a_\mu^{I=1}$. We thus do not expect IB corrections to dramatically shift the results for $a_\mu^{\text{sconn+disc}}$ or a_μ^{disc} obtained above. An

[6] A clear discussion of the SIB/EM separation issue can be found in Secs. 3.1.1 and 3.1.2 of the 2019 FLAG report [50].

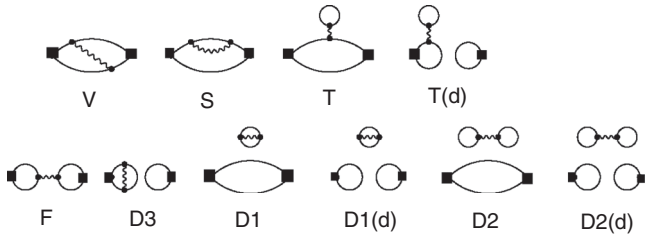

FIG. 1. Valence-valence (vv), valence-sea (vs), and sea-sea (ss) connected (c) and disconnected (d) graphs contributing to the full $I=1$, $I=0$, and MI EM contributions to $a_\mu^{\mathrm{LO,HVP}}$, following the RBC/UKQCD labeling scheme [14]. For a more detailed description, see the main text.

improved estimate of the IB corrections can be obtained as discussed below.

To first order in IB, SIB appears only in the mixed-isospin part of the EM polarization/EM spectral function. Thus, again to first order in IB, the IB contributions present in the physical versions of $a_\mu^{I=0}$ and $a_\mu^{I=1}$ are purely EM in nature. We need these only in an inclusive (sum over exclusive modes) form and will take advantage of details of the recent BMW lattice assessment of EM contributions to $a_\mu^{\mathrm{LO,HVP}}$ [20] to both show that these must be small and obtain actual estimates of their size, thereby confirming this expectation, as described in more detail below. We will then turn to the issue of the mixed-isospin contaminations present in the physical exclusive-mode contributions.

A. EM IB contributions

The diagrams producing $O(\alpha_{\mathrm{EM}})$ contributions to $\hat{\Pi}_{\mathrm{EM}}$, $\hat{\Pi}_{\mathrm{EM}}^{I=1}$, $\hat{\Pi}_{\mathrm{EM}}^{I=0}$, and $\hat{\Pi}_{\mathrm{EM}}^{\mathrm{MI}}$, and hence $O(\alpha_{\mathrm{EM}}^2)$ contributions to $a_\mu^{\mathrm{LO,HVP}}$, $a_\mu^{I=1}$, $a_\mu^{I=0}$, and a_μ^{MI}, are shown schematically in Fig. 1. The labeling follows the conventions of RBC/UKQCD [14]. The black squares denote external-current vertices. Gluon lines are not shown explicitly but are to be understood as connecting all quark lines in each diagram. The external-current couplings to a flavor $k=u$, d, s quark loop are c_k^a ($k=u$, d, s) if the external current is one of $J_\mu^{\mathrm{EM},a}$ ($a=3$ or 8) or $c_k^{\mathrm{EM}}=Q_k=c_k^3+c_k^8$, with Q_k the quark charge in units of e, if the external current is J_μ^{EM}. Since $\sum_{k=u,d,s} c_k^3=\sum_{k=u,d,s} c_k^8=\sum_{k=u,d,s} c_k^{\mathrm{EM}}=0$, diagrams containing a quark loop with only one vertex, whether of the external-current or internal-photon type, vanish in the flavor-$SU(3)$ [$SU(3)_F$] limit. Diagrams V, S, F, and $D1$ have no such suppression and survive in the $SU(3)_F$ limit. Diagrams T and $D3$ have a single such suppression, diagrams $T(d)$, $D1(d)$ and $D2$ a double suppression, and diagram $D2(d)$ a fourfold suppression. The contributions fall into valence-valence (vv), valence-sea (vs), and sea-sea (ss) subsets, with the double label specifying whether the internal-photon line connects two valence-quark lines, one valence- and one sea-quark line, or two sea-quark lines. These subsets can be further broken down into connected (c) and disconnected (d) parts that are characterized by whether the two external vertices lie on the same or on different quark loops. The (vv,c), (vv,d), (vs,c), (vs,d), (ss,c), and (ss,d) contributions are the sums of contributions from diagrams $V+S$, $F+D3$, T, $T(d)$, $D1+D2$, and $D1(d)+D2(d)$, respectively. Both (vv,c) diagrams are nonzero in the $SU(3)_F$ limit. The (vv,d) contribution is expected to be dominated by the unsuppressed diagram-F contribution and the (ss,c) contribution by the unsuppressed diagram-$D1$ contribution.[7] All other contributions, including the full (vs,c), (vs,d), and (ss,d) combinations, vanish in the $SU(3)_F$ limit.

BMW [20] has provided the following lattice results for the vv, vs, and ss connected and disconnected contributions to the full EM-current result, $a_\mu^{\mathrm{LO,HVP}}$:

$$\begin{aligned}
[a_\mu^{\mathrm{LO,HVP}}]_{(vv,c)} &= -1.23(40)(31)\times 10^{-10}\ \ (V+S),\\
[a_\mu^{\mathrm{LO,HVP}}]_{(vv,d)} &= -0.55(15)(10)\times 10^{-10}\ \ (F+D3),\\
[a_\mu^{\mathrm{LO,HVP}}]_{(vs,c)} &= -0.0093(86)(95)\times 10^{-10}\ \ (T),\\
[a_\mu^{\mathrm{LO,HVP}}]_{(vs,d)} &= 0.011(24)(14)\times 10^{-10}\ \ (T(d)),\\
[a_\mu^{\mathrm{LO,HVP}}]_{(ss,c)} &= 0.37(21)(24)\times 10^{-10}\ \ (D1+D2),\\
[a_\mu^{\mathrm{LO,HVP}}]_{(ss,d)} &= -0.040(33)(21)\times 10^{-10}\ \ (D1(d)+D2(d)).
\end{aligned} \tag{5.1}$$

The $SU(3)_F$-suppressed (vs,c), (vs,d), and (ss,d) contributions are a factor of $\sim$10 or more smaller than their $SU(3)_F$-unsuppressed counterparts, (vv,c), (vv,d), and (ss,c), suggesting a strong suppression in differences of light- and strange-quark-loop contributions, thus further supporting the expectation that diagram F will dominate the (vv,d) contribution and diagram $D1$ will dominate the (ss,c) contribution.

Based on this observation, we will, in what follows, neglect contributions which vanish in the $SU(3)_F$ limit and discuss the extent to which the BMW full-EM-current results can be broken down into their $I=1$, $I=0$, and MI components. Such a breakdown will allow us to estimate the desired EM contributions to a_μ^{MI} and $a_\mu^{\mathrm{sconn+disc}}=a_\mu^{I=0}-\frac{1}{9}a_\mu^{I=1}$.

It is useful to first introduce some notation for the loop contributions to the various subtracted polarizations from the unsuppressed diagrams of Fig. 1. It is convenient to explicitly factor out (i) both the external-current couplings and the internal-photon couplings (the latter in units of e) for diagrams V, S, and F and (ii) the external-current couplings for diagram $D1$. In a given lattice configuration,

[7]Diagrams F and $D1$ are $1/N_c$ suppressed, and the BMW results, indeed, show a suppression of the contributions from these diagrams relative to the $1/N_c$-unsuppressed $V+S$ contribution sum.

the loop contributions are determined by the quark propagators, which are in turn fixed by the gluon field configuration. The corresponding contributions to the subtracted polarizations are obtained by averaging over the ensemble. We define the "loop factor" for a given contribution as the full contribution divided (i) by the product of the relevant explicit external-current and internal-photon couplings for diagrams V, S, and F and (ii) by the product of the relevant explicit external-current couplings for diagram $D1$.[8] The following notation is employed for the loop factors of the $SU(3)_F$-unsuppressed contributions from the connected diagrams $\kappa = V$, S and $D1$ and disconnected diagram F:

(a) $L_j^{(\kappa)}$, $j = u, d, s$, denotes the flavor-j quark-loop factor for connected diagram $\kappa = V$, S. With this notation, the diagram-V contribution to $\hat{\Pi}_{\rm EM}$, for example, is

$$\sum_{k=u,d,s} Q_k^4 L_k^{(V)}, \tag{5.2}$$

where two factors of Q_k come from the external-current vertices and the remaining two come from the internal-photon vertices. Similarly, the diagram-V contribution to $\hat{\Pi}^{I=1}$ is

$$\sum_{k=u,d,s} (c_k^{\rm EM,3})^2 Q_k^2 L_k^{(V)}, \tag{5.3}$$

that to $\hat{\Pi}^{I=0}$ is

$$\sum_{k=u,d,s} (c_k^{\rm EM,8})^2 Q_k^2 L_k^{(V)}, \tag{5.4}$$

and that to $\hat{\Pi}^{\rm MI}$ is

$$2 \sum_{k=u,d,s} c_k^{\rm EM,3} c_k^{\rm EM,8} Q_k^2 L_k^{(V)}, \tag{5.5}$$

where the factor of 2 results from the presence of both $ab = 38$ and $ab = 83$ contributions.

(b) $LL_{k,m}^{(F)}$ denotes the loop factor for the two-disconnected-loop diagram-F contribution with a flavor-k quark loop attached to the left external vertex and a flavor-m quark loop attached to the right external vertex. This represents the ensemble average over the product of the two loops and does not factorize into a product of the ensemble averages of the individual loops. With this definition, the diagram-F contribution to $\hat{\Pi}_{\rm EM}$ is

$$\sum_{k,m=u,d,s} Q_k^2 Q_m^2 LL_{k,m}^{(F)}, \tag{5.6}$$

that to $\hat{\Pi}_{\rm EM}^{I=1}$ is

$$\sum_{k,m=u,d,s} c_k^{\rm EM,3} c_m^{\rm EM,3} Q_k Q_m LL_{k,m}^{(F)}, \tag{5.7}$$

that to $\hat{\Pi}_{\rm EM}^{I=0}$ is

$$\sum_{k,m=u,d,s} c_k^{\rm EM,8} c_m^{\rm EM,8} Q_k Q_m LL_{k,m}^{(F)}, \tag{5.8}$$

and that to $\hat{\Pi}_{\rm EM}^{\rm MI}$ is

$$2 \sum_{k,m=u,d,s} c_k^{\rm EM,3} c_m^{\rm EM,8} Q_k Q_m LL_{k,m}^{(F)}. \tag{5.9}$$

(c) $LL_k^{(D1)}$ denotes the loop factor for the two-disconnected-loop diagram-$D1$ contribution with a flavor-k quark loop attached to both external vertices, summed over all three flavors in the disconnected EM vacuum bubble. This again represents the ensemble average over the product of the two loops, and does not factorize into a product of the ensemble averages of the individual loops. With this definition, the diagram-$D1$ contribution to $\hat{\Pi}_{\rm EM}$ is

$$\sum_{k=u,d,s} Q_k^2 LL_k^{(D1)}, \tag{5.10}$$

that to $\hat{\Pi}_{\rm EM}^{I=1}$ is

$$\sum_{k=u,d,s} (c_k^{\rm EM,3})^2 LL_k^{(D1)}, \tag{5.11}$$

that to $\hat{\Pi}_{\rm EM}^{I=0}$ is

$$\sum_{k=u,d,s} (c_k^{\rm EM,8})^2 LL_k^{(D1)}, \tag{5.12}$$

and that to $\hat{\Pi}_{\rm EM}^{\rm MI}$ is

$$2 \sum_{k=u,d,s} c_k^{\rm EM,3} c_k^{\rm EM,8} LL_k^{(D1)}. \tag{5.13}$$

The $\hat{\Pi}_{\rm EM}$ contributions are, of course, in all cases the sums of the corresponding $\hat{\Pi}_{\rm EM}^{I=1}$, $\hat{\Pi}_{\rm EM}^{I=0}$, and $\hat{\Pi}_{\rm EM}^{\rm MI}$ contributions.

The associated contributions to $a_\mu^{\rm LO,HVP}$, $a_\mu^{I=1}$, $a_\mu^{I=0}$, and $a_\mu^{\rm MI}$ are obtained by integrating the relevant subtracted polarization with respect to Q^2 using the Euclidean-Q^2 weighting given in Eq. (2.11). Expressions for these contributions can be obtained from the corresponding expressions for the contributions to the subtracted polarizations by replacing the loop factors $L_k^{(\kappa)}$ ($\kappa = V$, S), $LL_{k,m}^{(F)}$, and $LL_k^{(D1)}$ with the correspondingly weighted integrals of these loop factors, which we denote by $\bar{L}_k^{(\kappa)}$ ($\kappa = V$, S), $\overline{LL}_{k,m}^{(F)}$, and $\overline{LL}_k^{(D1)}$ in what follows.

[8]The factors of e^2 coming from the two internal-photon vertices and the relevant internal-photon propagators are thus, in all cases, absorbed into the definitions of the corresponding loop factors.

With this notation, the breakdowns for the $SU(3)_F$-unsuppressed contributions of diagrams V, S, F, and $D1$ proceed as follows, where we take into account the fact that the resulting decomposition is to be applied to the BMW results for the full $a_\mu^{\rm LO,HVP}$ (vv,c), (vv,d), and (ss,c) contributions and that those results were obtained as corrections evaluated using isospin-symmetric configurations. Since all relevant flavor-dependent coupling factors were explicitly factored out in defining the loop factors for the subtracted polarizations above, one has $L_u^{(\kappa)} = L_d^{(\kappa)} \equiv L_\ell^{(\kappa)}$ for the diagram $\kappa = V, S$ loop factors, $LL_u^{(D1)} = LL_d^{(D1)}$ for the diagram-$D1$ loop factors, and $LL_{u,u}^{(F)} = LL_{u,d}^{(F)} = LL_{d,u}^{(F)} = LL_{u,u}^{(F)} \equiv LL_{\ell,\ell}^{(F)}$ and $LL_{u,s}^{(F)} = LL_{d,s}^{(F)} = LL_{s,u}^{(F)} = LL_{s,d}^{(F)} \equiv LL_{\ell,s}^{(F)}$ for the diagram-F loop factors, with similar relations for the integrated loop factors $\bar{L}_k^{(\kappa)}$, $\overline{LL}_k^{(D1)}$, and $\overline{LL}_{k,m}^{(F)}$.

Since diagrams V and S share the same products of external-current and internal-photon coupling factors, it is also convenient to define the combined $V+S \equiv (vv,c)$ loop factors,

$$\bar{L}_k^{(vv,c)} \equiv \bar{L}_k^{(V)} + \bar{L}_k^{(S)}. \tag{5.14}$$

We also introduce the $SU(3)_F$-breaking ratios

$$\begin{aligned} x_{(vv,c)} &\equiv \bar{L}_s^{(vv,c)}/\bar{L}_\ell^{(vv,c)}, \\ x_{D1} &\equiv \overline{LL}_s^{(D1)}/\overline{LL}_\ell^{(D1)}, \\ x_F &\equiv \overline{LL}_{\ell,s}^{(F)}/\overline{LL}_{\ell,\ell}^{(F)}, \\ y_F &\equiv \overline{LL}_{s,s}^{(F)}/\overline{LL}_{\ell,\ell}^{(F)} \end{aligned} \tag{5.15}$$

for use in the expressions below. These ratios are all, of course, equal to 1 in the $SU(3)_F$ limit.[9]

With this notation established, one finds the following bounds:

(a) For the (vv,c) (diagrams $V+S$) sum,

$$\begin{aligned} [a_\mu^{\rm LO,HVP}]_{(vv,c)} &= [17\bar{L}_\ell^{(vv,c)} + \bar{L}_s^{(vv,c)}]/81, \\ [a_\mu^{I=1}]_{(vv,c)} &= 5\bar{L}_\ell^{(vv,c)}/36, \\ [a_\mu^{I=0}]_{(vv,c)} &= [5\bar{L}_\ell^{(vv,c)} + 4\bar{L}_s^{(vv,c)}]/324, \\ [a_\mu^{\rm MI}]_{(vv,c)} &= [\bar{L}_\ell^{(vv,c)}]/18. \end{aligned} \tag{5.16}$$

The combinations of interest, $[a_\mu^{\rm sconn+disc}]_{(vv,c)}$ and $[a_\mu^{\rm MI}]_{(vv,c)}$, thus represent the fractions

$$\begin{aligned} [a_\mu^{\rm sconn+disc}]_{(vv,c)}/[a_\mu^{\rm LO,HVP}]_{(vv,c)} &= \frac{1}{17}\frac{x_{(vv,c)}}{1+(x_{(vv,c)}/17)}, \\ [a_\mu^{\rm MI}]_{(vv,c)}/[a_\mu^{\rm LO,HVP}]_{(vv,c)} &= \frac{9}{34}\frac{1}{1+(x_{(vv,c)}/17)} \end{aligned} \tag{5.17}$$

of the BMW (vv,c) total $-1.23(40)(31)\times 10^{-10}$. The cancellation of the terms proportional to $\bar{L}_\ell^{(vv,c)}$ is a generic feature of the (vv,c) contribution $[a_\mu^{\rm sconn+disc}]_{(vv,c)}$, and it produces a sizable numerical suppression of this contribution relative to the full (vv,c) sum. If we consider the (presumably conservative) range $0 \le x_{(vv,c)} \le 1$, we see that $[a_\mu^{\rm sconn+disc}]_{(vv,c)}$ should lie somewhere between 0 and $1/18$ times the full BMW (vv,c) result, i.e., in the range

$$-0.068(22)(17)\times 10^{-10} \le [a_\mu^{\rm sconn+disc}]_{(vv,c)} \le 0, \tag{5.18}$$

and hence should produce an essentially negligible correction to the strange-quark-connected plus disconnected and disconnected results of Eqs. (4.12) and (4.14). For the same range of $x_{(vv,c)}$, the mixed-isospin (vv,c) contribution lies in the range between $9/34$ and $1/4$ times the full (vv,c) result, i.e., in the rather precisely determined range

$$\begin{aligned} &-0.326(106)(82)\times 10^{-10} \le [a_\mu^{\rm MI}]_{(vv,c)} \\ &\quad \le -0.308(100)(78)\times 10^{-10}. \end{aligned} \tag{5.19}$$

(b) For the (vv,d) contribution, neglecting the $SU(3)_F$-suppressed diagram-$D3$ contribution, we have

[9]Note that $SU(3)$ breaking for these quantities can be larger than naively expected since the weight in the dispersive representation strongly emphasizes the low-s part of the spectrum. $SU(3)$ breaking in the subtracted polarizations (related to the spectral functions by the usual subtracted dispersion relation) can then be further enhanced by "kinematic" effects associated with the shift to higher s in the spectrum (and hence to reduced dispersive weight) of states which couple to the strange current compared to those which couple to the nonstrange current. An example is provided by the relation between the strange- and light- (ud) connected components of the isospin-limit contributions to $a_\mu^{\rm LO,HVP}$. Using C to denote the corresponding connected diagram (diagram $D1$ without the EM vacuum bubble), one has $[a_\mu^{\rm LO,HVP}]_C = [5\bar{L}_\ell^{(C)} + \bar{L}_s^{(C)}]/9$. In the $SU(3)_F$ limit, where $x_C \equiv \bar{L}_s^{(C)}/\bar{L}_\ell^{(C)} = 1$, the light-connected contribution is thus a factor of 5 larger than the strange-quark-connected contribution, while for physical m_s and m_ℓ this ratio is $\sim$12.2 [29], which corresponds to $x_C \simeq 0.41$.

$$
\begin{aligned}
[a_\mu^{\mathrm{LO,HVP}}]_{(vv,d)} &= [25\overline{LL}^{(F)}_{\ell,\ell} + 10\overline{LL}^{(F)}_{\ell,s} + \overline{LL}^{(F)}_{s,s}]/81, \\
[a_\mu^{I=1}]_{(vv,d)} &= \overline{LL}^{(F)}_{\ell,\ell}/4, \\
[a_\mu^{I=0}]_{(vv,d)} &= [\overline{LL}^{(F)}_{\ell,\ell} + 4\overline{LL}^{(F)}_{\ell,s} + 4\overline{LL}_{s,s}]/324, \\
[a_\mu^{\mathrm{MI}}]_{(vv,d)} &= [\overline{LL}^{(F)}_{\ell,\ell} + 2\overline{LL}^{(F)}_{\ell,s}]/18. \qquad (5.20)
\end{aligned}
$$

The combinations of interest, $[a_\mu^{\mathrm{sconn+disc}}]_{(vv,d)}$ and $[a_\mu^{\mathrm{MI}}]_{(vv,d)}$, then represent fractions

$$
\begin{aligned}
[a_\mu^{\mathrm{sconn+disc}}]_{(vv,d)}/[a_\mu^{\mathrm{LO,HVP}}]_{(vv,d)} &= -\left[\frac{2-x_F-y_F}{25+10x_F+y_F}\right], \\
[a_\mu^{\mathrm{MI}}]_{(vv,d)}/[a_\mu^{\mathrm{LO,HVP}}]_{(vv,d)} &= \frac{9}{2}\left[\frac{1+2x_F}{25+10x_F+y_F}\right] \qquad (5.21)
\end{aligned}
$$

of the BMW (vv,d) total, $-0.55(15)(10)\times 10^{-10}$. There is a strong cancellation [exact in the $SU(3)_F$ limit] for the strange-quark-connected plus disconnected combination. If we once more assume the joint range $0 \le x_F \le 1$, $0 \le y_F \le 1$ to represent a conservative choice, $[a_\mu^{\mathrm{sconn+disc}}]_{(vv,d)}$ is expected to lie somewhere between $-2/25$ and 0 times the full BMW (vv,d) result, i.e., in the range

$$
0 \le [a_\mu^{\mathrm{sconn+disc}}]_{(vv,d)} \le 0.044(12)(8)\times 10^{-10}, \qquad (5.22)
$$

and hence to again produce an essentially negligible correction to the strange-quark-connected plus disconnected and disconnected results, Eqs. (4.12) and (4.14). For the same joint x_F, y_F range, the mixed-isospin (vv,d) contribution lies between $9/52$ and $27/70$ times the full (vv,d) result, i.e., in the range

$$
\begin{aligned}
&-0.212(58)(39)\times 10^{-10} \le [a_\mu^{\mathrm{MI}}]_{(vv,d)} \\
&\quad \le -0.095(26)(17)\times 10^{-10}. \qquad (5.23)
\end{aligned}
$$

(c) For the (ss,c) contribution, neglecting the doubly $SU(3)_F$-suppressed diagram-$D2$ contribution, we have

$$
\begin{aligned}
[a_\mu^{LO,HVP}]_{(ss,c)} &= [5\overline{LL}^{(D1)}_{\ell} + \overline{LL}^{(D1)}_{s}]/9, \\
[a_\mu^{I=1}]_{(ss,c)} &= \overline{LL}^{(D1)}_{\ell}/2, \\
[a_\mu^{I=0}]_{(ss,c)} &= [\overline{LL}^{(D1)}_{\ell} + 2\overline{LL}^{(D1)}_{s}]/18, \\
[a_\mu^{\mathrm{MI}}]_{(ss,c)} &= 0. \qquad (5.24)
\end{aligned}
$$

The combinations of interest, $[a_\mu^{\mathrm{sconn+disc}}]_{(ss,c)}$ and $[a_\mu^{\mathrm{MI}}]_{(ss,c)}$, thus represent the fractions

$$
\begin{aligned}
[a_\mu^{\mathrm{sconn+disc}}]_{(ss,c)}/[a_\mu^{\mathrm{LO,HVP}}]_{(ss,c)} &= \frac{1}{5}\frac{x_{D1}}{1+(x_{D1}/5)}, \\
[a_\mu^{\mathrm{MI}}]_{(ss,c)}/[a_\mu^{\mathrm{LO,HVP}}]_{(ss,c)} &= 0 \qquad (5.25)
\end{aligned}
$$

of the BMW (ss,c) total $0.37(21)(24)\times 10^{-10}$. Considering the (presumably conservative) range $0 \le x_{D1} \le 1$, $[a_\mu^{\mathrm{sconn+disc}}]_{(ss,c)}$ is thus expected to lie somewhere between 0 and $1/6$ times the full BMW (ss,c) result, i.e., in the range

$$
0 \le [a_\mu^{\mathrm{sconn+disc}}]_{(ss,c)} \le 0.062(35)(40)\times 10^{-10}, \qquad (5.26)
$$

once more producing an essentially negligible correction to the strange-quark-connected plus disconnected and disconnected results, Eqs. (4.12) and (4.14).

If we combine the BMW-induced statistical and systematic errors in quadrature, the (vv,c), (vv,d), and (ss,c) contributions to the strange-quark-connected plus disconnected sum lie in the ranges $(-0.068(28)\times 10^{-10}, 0)$, $(0, 0.044(14)\times 10^{-10})$, and $(0, 0.062(53)\times 10^{-10})$, respectively. When we add the errors in these quantities linearly, the sum of the three contributions lies between $-0.068(28)\times 10^{-10}$ and $0.106(67)\times 10^{-10}$, or, at the 1σ level, in the interval $(-0.096\times 10^{-10}, 0.173\times 10^{-10})$, leading to a conservative final assessment of

$$
[a_\mu^{\mathrm{sconn+disc}}]_{(vv,c)+(vv,d)+(ss,c)} = 0.04(13)\times 10^{-10}. \qquad (5.27)
$$

The central value and error on the associated correction to the strange-quark-connected plus disconnected result, Eq. (4.12), and hence also the disconnected result, Eq. (4.14), are thus both entirely negligible on the scale of the errors in those results.

A similar treatment of the BMW errors and (vv,c) and (vv,d) uncertainty ranges produces an estimate for the EM contribution to a_μ^{MI} which, at the 1σ level, lies in the interval $(-0.742\times 10^{-10}, -0.245\times 10^{-10})$, leading to a conservative final assessment of

$$
[a_\mu^{\mathrm{MI}}]_{(vv,c)+(vv,d)+(ss,c)} = -0.49(25)\times 10^{-10}. \qquad (5.28)
$$

This result, like that of Eq. (5.27), is inclusive from the dispersive point of view. Unlike that earlier result, however, it cannot be used to remove the associated, mixed-isospin component of the EM contribution to the IB-uncorrected strange-quark-connected plus disconnected result Eq. (4.12) or disconnected result Eq. (4.14). The reason is that the nominally $I=0$ (G-parity-negative) and $I=1$ (G-parity-positive) exclusive-mode contributions to the inclusive sum in Eq. (5.28) enter the difference underlying the results of Eqs. (4.12) and (4.14) with different signs. To correct for the mixed-isospin contamination of the nominal $I=0$ and $I=1$ sums, one thus needs to understand the breakdown of the

mixed-isospin contribution into its exclusive-mode components. This issue is discussed in Sec. V B.

B. The mixed-isospin correction

As is the case for the dominant isospin-conserving (IC) contribution, we expect the IB contributions to $a_\mu^{\rm LO,HVP}$ to be dominated by contributions from the region of the lowest-lying (ρ, ω) resonances, doubly so since IB contributions in this region are subject to enhancements generated by the impact on the effects of ρ-ω interference of the smallness of the ρ-ω mass difference. In this region, the mixed-isospin spectral contribution, $\rho_{\rm EM}^{\rm MI}(s)$, will appear essentially entirely in the 2π and 3π exclusive modes.

Unlike the $ab = 33, 88$ components, which to first order in IB receive only EM IB contributions, the mixed-isospin component contains both SIB and EM IB contributions. Equation (5.28) provides an estimate for the latter in the EM/SIB separation convention used by BMW. Two determinations, one continuum chiral perturbation theory based, the other lattice based, exist for the corresponding SIB component. The results, $a_\mu^{SIB} = 3.32(89) \times 10^{-10}$ [51] and $1.93(1.20) \times 10^{-10}$ [20], respectively, are compatible within errors, with a naive average of $2.83(71) \times 10^{-10}$. The lattice result is subject to the strong cancellation between connected and disconnected contributions anticipated in Ref. [21]. Both SIB results are inclusive from the dispersive point of view. Combining, for example, the EM and continuum SIB estimates produces an estimate of $2.8(9) \times 10^{-10}$ for the full EM + SIB inclusive mixed-isospin contribution $a_\mu^{\rm MI}$. Employing instead the naive average of the continuum and lattice SIB results yields the somewhat smaller value $2.3(8) \times 10^{-10}$.

The ρ-ω region 2π and 3π IB contributions to $a_\mu^{\rm LO,HVP}$ can be estimated from the interference terms in fits to the $e^+e^- \to 2\pi$ and $e^+e^- \to 3\pi$ electroproduction cross sections associated with the IB $e^+e^- \to \omega \to 2\pi$ and $e^+e^- \to \rho \to 3\pi$ contributions to the amplitudes appearing in those fits. These contributions, to first order in IB, lie entirely in the mixed-isospin contribution, $a_\mu^{\rm MI}$.

The mixed-isospin EM + SIB 2π contribution is taken from a fit to the 2π cross section based on the dispersively constrained form for the timelike π form factor detailed in Ref. [52]. The parameter ϵ_ω entering that form, which parametrizes the ρ-ω region IB, is expected to have a small nonzero phase [53]. Colangelo *et al.* [52] recently performed a fit to existing $e^+e^- \to 2\pi$ cross section data while including this phase as a free parameter. This fit produces a result of $\sim 4°$ for the phase, and a corresponding IB $a_\mu^{\rm MI}$ contribution of $\sim 3.65 \times 10^{-10}$ [54]. Although the fitted phase is small, the result for this contribution is sensitive to the inclusion of the phase in the fit, for the reason explained in Ref. [55]. The same fit, with the phase fixed to zero by hand, instead gives an IB 2π contribution of $\sim 4.32 \times 10^{-10}$ [54]. Given this sensitivity, we take the $\sim 0.67 \times 10^{-10}$ difference between the results of the free-phase and no-phase fits as an estimate of the uncertainty on the mixed-isospin IB, 2π contribution to $a_\mu^{\rm MI}$.

The mixed-isospin EM + SIB ρ-ω region 3π contribution is estimated using the results of vector meson dominance (VMD)-based fits to recent *BABAR* $e^+e^- \to 3\pi$ cross-section data, which were reported in Ref. [56] and which show strong evidence for an IB $\rho \to 3\pi$ interference contribution. The $a_\mu^{\rm MI}$ contribution produced by the interference term in the preferred version of this fit is $-0.56(12) \times 10^{-10}$ [57]. The error here does not account for possible additional model dependence associated with the use of VMD for the IC and IB contributions to the amplitude.

It is worth noting that, in spite of resonant enhancement, the magnitudes of the mixed-isospin, ρ-ω region exclusive-mode IB 2π and 3π contributions do not exceed the naive $\lesssim 1\%$ estimate for the size of IB relative to IC contributions. The sum of these contributions, $3.1(7) \times 10^{-10}$, is, moreover, compatible within errors with the sum of the results quoted above for the sum of inclusive EM and SIB contributions to $a_\mu^{\rm MI}$ [$2.8(9) \times 10^{-10}$ if one uses the continuum version of the SIB contribution, $2.3(8) \times 10^{-10}$ if one uses the naive average of the continuum and lattice results], confirming the expectation that $a_\mu^{\rm MI}$ will be dominated by 2π and 3π exclusive-mode contributions. The errors, however, are large enough to accommodate small additional contributions from the remaining, higher-s exclusive modes. With $K\bar{K}$ and 4π contributions strongly dominating the sum of the remaining nominal $I = 0$ and $I = 1$ contributions to $a_\mu^{\rm LO,HVP}$, we expect the magnitudes of the additional mixed-isospin corrections to the nominal $I = 0$ and $I = 1$ sums to be $\lesssim 1\%$ of the corresponding exclusive-mode contributions, i.e., $\lesssim 0.01[a_\mu^{\rm LO,HVP}]_{K\bar{K}}$ ($\lesssim 0.36 \times 10^{-10}$) and $\lesssim 0.01[a_\mu^{\rm LO,HVP}]_{4\pi}$ ($\lesssim 0.34 \times 10^{-10}$), respectively. Even if these were to enter the correction to the nominal $a_\mu^{I=0} - \frac{1}{9} a_\mu^{I=1}$ combination with the same sign, the resulting correction to this combination would be $\lesssim 0.4 \times 10^{-10}$. We will thus assign an additional 0.4×10^{-10} uncertainty to the mixed-isospin correction to account for the missing mixed-isospin IB corrections associated with exclusive modes other than 2π and 3π.

C. The final IB correction

The estimates for the isospin-limit strange-quark-connected plus disconnected contributions to $a_\mu^{\rm LO,HVP}$, Eqs. (4.12) and (4.14), were obtained by assigning the full exclusive-mode 2π contribution to $a_\mu^{I=1}$ and the full exclusive-mode 3π contribution to $a_\mu^{I=0}$. As discussed above, these exclusive-mode contributions contain small IB contaminations which in fact belong to $a_\mu^{\rm MI}$ rather than to $a_\mu^{I=1}$ or $a_\mu^{I=0}$. These contaminations produce an associated small

mixed-isospin IB contamination of the nominal $a_\mu^{I=0} - \frac{1}{9}a_\mu^{I=1}$ combination obtained above. When we take the estimates just obtained for the mixed-isospin 2π and 3π contaminations and the bound on possible mixed-isospin contaminations from other exclusive modes, the mixed-isospin contamination to be subtracted from the result of Eq. (4.14) to obtain the true isospin-limit strange-quark-connected plus disconnected contribution to $a_\mu^{\rm LO,HVP}$ is

$$-0.56(12)\times 10^{-10} - \frac{1}{9}(3.65(67)\times 10^{-10}) \pm 0.4\times 10^{-10} = -0.97(14)(40)\times 10^{-10}, \quad (5.29)$$

where the first error on the final result is the quadrature sum of those on the first two terms on the lhs and the second reflects the estimate above for possible contributions from non 2π and non 3π exclusive modes.

Subtracting the result (5.29) from the IB-uncorrected nominal results $a_\mu^{\rm sconn+disc} = 39.1(1.4)\times 10^{-10}$ and $a_\mu^{\rm disc} = -14.3(1.4)\times 10^{-10}$ of Eqs. (4.12) and (4.14), we obtain our final IB-corrected isospin-limit results,

$$a_\mu^{\rm sconn+disc} = 40.1(1.4)(0.4)\times 10^{-10}, \qquad a_\mu^{\rm disc} = -13.3(1.4)(0.4)\times 10^{-10}. \quad (5.30)$$

VI. AN ALTERNATE ANALYSIS USING RESULTS FROM REFERENCE [28]

A determination of exclusive-mode contributions to $a_\mu^{\rm LO,HVP}$ similar to that of Refs. [26,27] was carried out in Ref. [28], which we will refer to as DHMZ. The analysis above can thus be repeated using DHMZ input and the results compared to those obtained using KNT2019 input.

DHMZ's exclusive-mode results are somewhat less well suited to our purpose than are KNT2019's, for the following reasons. First, where the dispersive exclusive-mode $a_\mu^{\rm LO,HVP}$ contributions tabulated in KNT2019 correspond to contributions from threshold to $s = (1.937\ {\rm GeV})^2 = 3.752\ {\rm GeV}^2$, those in DHMZ correspond to contributions only up to $s = (1.8\ {\rm GeV})^2 = 3.24\ {\rm GeV}^2$. The pQCD approximation must thus be used to lower s in a DHMZ-based analysis than in a KNT2019-based one. Since $R(s)$ shows a clear DV dip below perturbative expectations in the region between 3.24 and $3.752\ {\rm GeV}^2$, this makes a DHMZ-based analysis potentially more sensitive to DV corrections, which can be only roughly estimated at present. Second, the exclusive-mode $R(s)$ contributions and covariances underlying the DHMZ exclusive-mode $a_\mu^{\rm LO,HVP}$ contribution results are not publicly available, unlike the corresponding KNT2019 results, which are available from Keshavarzi *et al.* [27] upon request. The access to KNT2019's exclusive-mode data allows us to perform the internally self-consistent hybrid τ-KNT2019-electroproduction determination of the $K\bar{K}$ contribution to $a_\mu^{\rm sconn+disc}$ described above. The lack of access to the corresponding DHMZ exclusive-mode cross sections and covariances means an analogous, fully self-consistent DHMZ-based determination of that contribution is not possible. We have thus been forced to use a KNT2019-based determination of the $I=1$ $K\bar{K}$ contribution from the region between 2.7556 and $3.24\ {\rm GeV}^2$ to determine the full hybrid τ-electroproduction $I=1$ DHMZ-exclusive-mode-region $K\bar{K}$ contribution, combining that with the DHMZ result for the full $I=0+1$ $K\bar{K}$ contribution up to $3.24\ {\rm GeV}^2$, to determine the "DHMZ-based" $K\bar{K}$ contribution to $a_\mu^{\rm sconn+disc}$.

While the use of DHMZ input has some minor disadvantages, it is of interest to pursue the alternate, DHMZ-based determination of $a_\mu^{\rm sconn+disc}$ and $a_\mu^{\rm disc}$ since KNT2019 and DHMZ, despite analyzing essentially identical electroproduction cross-section data, obtain somewhat discrepant results for a number of exclusive-mode $a_\mu^{\rm LO,HVP}$ contributions (the situation is discussed in more detail in Sec. 2.3.5 of Ref. [29], with Table 5 providing a summary of the main discrepancies). Such discrepancies exist for both nominally $I=0$ and nominally $I=1$ exclusive-mode contributions and have the potential to affect the weighted difference of $I=0$ and $I=1$ contributions which determines $a_\mu^{\rm sconn+disc}$.

The implementation of the DHMZ-based analysis follows exactly that of the KNT2019-based analysis detailed above. DHMZ results for the various exclusive-mode $a_\mu^{\rm LO,HVP}$ contributions are taken from Table 2 of DHMZ.[10] Conversions of G-parity-ambiguous-mode $a_\mu^{\rm LO,HVP}$ contributions to the corresponding $a_\mu^{\rm sconn+disc}$ contributions proceed exactly as in the case of the KNT2019-based analysis, with the exception of the $K\bar{K}$ mode, where, as noted above, we do not have access to the DHMZ $K\bar{K}$ exclusive-mode cross sections and covariances, and hence have used KNT2019 results for these quantities to determine the $K\bar{K}$ contribution to $a_\mu^{\rm LO,HVP}$ from the region $2.7556\ {\rm GeV}^2 \le s \le 3.24\ {\rm GeV}^2$.

The results of the DHMZ-based analysis are as follows. The sums of the nominally $I=1$ (G-parity-positive) and

[10]The reader is reminded that results tabulated in KNT2019 and DHMZ, though having the same exclusive-mode labelings, are different, corresponding to contributions from different ranges of s (for DHMZ up to $s = 3.24\ {\rm GeV}^2$, for KNT2019 up to $s = 3.752\ {\rm GeV}^2$), and thus should not be compared mode by mode. A comparison of contributions for a subset of exclusive modes over the common DHMZ range $s \le 3.24\ {\rm GeV}^2$ is provided in Table 5 of Ref. [29]. The lower DHMZ upper end point, which lies below the $p\bar{p}$ threshold, also means that there are no DHMZ analogs of the KNT2019 entries for the G-parity-ambiguous $p\bar{p}$ and $n\bar{n}$ mode contributions.

$I = 0$ (G-parity-negative) exclusive-mode contributions from Table 2 of DHMZ are $542.74(84)(3.28)(1.12) \times 10^{-10}$ and $53.65(42)(1.11)(1.02) \times 10^{-10}$, respectively, where the errors are, in order, the statistical, mode-specific mode-to-mode-uncorrelated systematic and the 100% correlated common systematic error components of Ref. [28]. When the first two errors are combined in quadrature, these results become $542.74(3.39)(1.12) \times 10^{-10}$ and $53.65(1.18)(1.02) \times 10^{-10}$, respectively.

For the $K\bar{K}$ mode, the $I = 1$ contribution to $a_\mu^{\mathrm{LO,HVP}}$ from the region $s \leq 2.7556\ \mathrm{GeV}^2$ is obtained, as before, using the *BABAR* τ data [25]. The result, $0.764(33) \times 10^{-10}$, is thus unchanged. The KNT2019 input produces a maximally conservative estimate of $0.070(70) \times 10^{-10}$ for the $I = 1$ contribution from the region $2.7556\ \mathrm{GeV}^2 \leq s \leq 3.24\ \mathrm{GeV}^2$. The resulting $s \leq 3.24\ \mathrm{GeV}^2$, $I = 1$ contribution, $0.834(34) \times 10^{-10}$, combined with the DHMZ two-mode $K\bar{K}$ $I = 0 + 1$ contribution total, then yields $[a_\mu^{\mathrm{sconn+disc}}]_{K\bar{K}} = 34.98(43)(36)$, where the second error is the (linear) sum of the 100% correlated common systematic DHMZ errors in the K^+K^- and K_SK_L contributions.

For the $K\bar{K}\pi$ mode, using the results for the $I = 1$ component of the observed cross sections obtained by *BABAR* [40], one finds an $I = 1$ contribution to $a_\mu^{\mathrm{LO,HVP}}$ from the region $s \leq 3.24\ \mathrm{GeV}^2$ of $0.664(34)(105) \times 10^{-10}$, where the first error is statistical and the second systematic. Combining these errors in quadrature, the DHMZ result for the full $I = 0 + 1$ contribution then implies that $[a_\mu^{\mathrm{sconn+disc}}]_{K\bar{K}\pi} = 1.71(17)(6)$, where the second error is again the 100% correlated common systematic error on the DHMZ $K\bar{K}\pi$ total.

For the $K\bar{K}2\pi$ mode, the $s \leq 3.24\ \mathrm{GeV}^2$, $I = 0$ $\phi(\to K\bar{K})\pi\pi$ contribution implied by *BABAR* $e^+e^- \to \phi\pi\pi$ cross-section results [58] is $0.117(8) \times 10^{-10}$. Subtracting this from the DHMZ $I = 0 + 1$ $K\bar{K}2\pi$ total and performing the usual maximally conservative treatment of the resulting G-parity-ambiguous residual, one finds that $[a_\mu^{\mathrm{sconn+disc}}]_{K\bar{K}2\pi} = 0.44(41)(0)$, where the second error is, once more, the 100% correlated common systematic DHMZ one.

For the remaining [$\omega K\bar{K}$ and $\eta K\bar{K}(\mathrm{no}\phi)$] DHMZ G-parity-ambiguous modes, the maximally conservative treatment of the sum of contributions from these modes yields a contribution of $0.00(1)(0) \times 10^{-10}$ to $a_\mu^{\mathrm{sconn+disc}}$, with the second error again the 100% correlated common systematic DHMZ one.

Finally, the five-loop-truncated pQCD estimate for the contribution to $a_\mu^{\mathrm{sconn+disc}}$ from the DHMZ inclusive region, $s > 3.24\ \mathrm{GeV}^2$ is found to be 7.28×10^{-10}, with, as above, negligible input-α_s and five-loop-truncation uncertainties.

Combining these results, we find for our DHMZ-based determination of the (pre-IB-corrected) strange-quark-connected plus disconnected sum

$$\begin{aligned} a_\mu^{\mathrm{sconn+disc}} &= \left[53.65(1.18)(1.02)_{\mathrm{lin}} - \frac{542.73(3.39)(1.12)_{\mathrm{lin}}}{9} + 34.98(43)(36)_{\mathrm{lin}}\right. \\ &\quad \left. + 1.71(17)(6)_{\mathrm{lin}} + 0.44(41)(1)_{\mathrm{lin}} + 0.00(1)(0)_{\mathrm{lin}} + 7.28\right] \times 10^{-10} \\ &= 37.76(1.39)(1.33)_{\mathrm{lin}} \times 10^{-10}, \end{aligned} \tag{6.1}$$

where the 100% correlated common systematic errors are identified by the subscript "lin". The first error in the final expression in Eq. (6.1) is the quadrature sum of the statistical and uncorrelated mode-specific systematic errors, while the second error is the linear sum of the 100% correlated common systematic errors. This treatment of the common systematic errors is that specified in Ref. [28].

Comparing Eqs. (4.12) and (6.1), we see (a) that the DHMZ-based value is 1.32×10^{-10} lower than the KNT2019-based value, and (b) that the DHMZ-based total error is more conservative. Using the naive average of the white paper strange-quark-connected result [29] and the BMW strange-quark-connected result [20], we find for our initial (pre-IB-corrected) DHMZ-based disconnected contribution the value $-15.61(1.39)(1.33)_{\mathrm{lin}} \times 10^{-10}$, which is to be compared to Eq. (4.14).

Finally, applying the IB corrections worked out in Sec. V, we arrive at

$$\begin{aligned} a_\mu^{\mathrm{sconn+disc}} &= 38.7(1.4)(1.3)_{\mathrm{lin}}(0.4) \times 10^{-10}, \\ a_\mu^{\mathrm{disc}} &= -14.6(1.4)(1.3)_{\mathrm{lin}}(0.4) \times 10^{-10}, \end{aligned} \tag{6.2}$$

where the third error has the same origin as the second error in Eq. (5.30).

Table II compares our isospin-symmetric results for $a_\mu^{\mathrm{sconn+disc}}$ and a_μ^{disc} to those of recent lattice studies that report results for both. Our disconnected results are seen to be in excellent agreement with all lattice results except that of the Mainz collaboration [18],[11] with which they are

[11]The result in Ref. [18] was obtained via an extrapolation to the physical point from results at heavier-than-physical pion masses, unlike the results obtained by the other collaborations.

TABLE II. Comparison of our results with recent lattice results for the isospin-limit three-flavor disconnected and strange-quark-connected plus full three-flavor disconnected contributions to $a_\mu^{\mathrm{LO,HVP}}$. The first and second errors in the lattice entries, shown in the upper half of the table, are statistical and systematic, respectively. Errors in the KNT2019- and DHMZ-based results of Eqs. (5.30) and (6.2), shown in the second-to-last and last lines of the lower half of the table, respectively, are as described in the text.

Source	n_f	$a_\mu^{\mathrm{disc}} \times 10^{10}$	$a_\mu^{\mathrm{sconn+disc}} \times 10^{10}$
RBC/UKQCD [4,11]	$2+1$	$-11.2(3.3)(2.3)$	$42.0(3.3)(2.3)$
BMW [9]	$2+1+1$	$-12.8(1.1)(1.6)$	$40.9(1.2)(1.7)$
Mainz [18]	$2+1$	$-23.2(2.2)(4.5)$	$31.3(3.3)(4.5)$
BMW [20]	$2+1+1$	$-13.36(1.18)(1.36)$	$40.03(1.18)(1.36)$
This work, Eq. (5.30)	$2+1$	$-13.3(1.4)(0.4)$	$40.1(1.4)(0.4)$
This work, Eq. (6.2)	$2+1$	$-14.6(1.4)(1.3)_{\mathrm{lin}}(0.4)$	$38.7(1.4)(1.3)_{\mathrm{lin}}(0.4)$

clearly incompatible. The errors in the results for a_μ^{disc} in Eqs. (5.30) and (6.2) are competitive with those of the most precise of the current lattice results [20]—and obtained at a dramatically reduced numerical cost.

VII. DISCUSSION

The main observations in this paper are (i) that a rather precise determination of $a_\mu^{\mathrm{sconn+disc}}$, the strange-quark-connected plus full three-flavor quark-disconnected contribution to $a_\mu^{\mathrm{LO,HVP}}$, can be obtained from electroproduction data and (ii) that, using lattice results for the strange-quark-connected contribution, this can be converted into a determination of the disconnected part, avoiding the direct calculation of the disconnected part on the lattice. While a completely lattice-based evaluation of $a_\mu^{\mathrm{LO,HVP}}$ is of great interest, this disconnected part is computationally expensive, and a "hybrid" approach, in which the disconnected part is obtained from experimental data and the connected part from the lattice, is of interest as well. Moreover, as mentioned in Sec. I, it is useful to compare results for different contributions to $a_\mu^{\mathrm{LO,HVP}}$ obtained using dispersive and lattice approaches.

It is worth reminding the reader that, to make contact with the disconnected contributions calculated on the lattice, our results for a_μ^{disc} are isospin-symmetric ones. This means that the EM disconnected contributions shown in Fig. 1 still have to be added to obtain a complete result for $a_\mu^{\mathrm{LO,HVP}}$. Since these corrections are much smaller than the isospin-symmetric disconnected contribution, however, it suffices, at a given level of overall precision, to evaluate them on the lattice with much larger relative errors.

While one of our two main observations is that the full three-flavor, isospin-symmetric disconnected contribution to $a_\mu^{\mathrm{LO,HVP}}$ can be obtained without the need of any disconnected lattice calculations, we did use some disconnected results (notably, the BMW results for diagrams F and $D1$ in Fig. 1) in our discussions of IB corrections in Sec. V. We stress, however, that although BMW input was used, the specifics of that input were not, in fact, numerically relevant, for the following reasons. First, the BMW EM results were not needed for the mixed-isospin EM corrections, where (i) the dominant combined SIB + EM 2π and 3π exclusive-mode contributions from the ρ-ω region were taken from experiment and (ii) since (in spite of the enhancement of these IB contributions from the rather small ρ-ω mass difference) these contributions are each $\sim$1% of the total IC contributions from these modes, it should be quite safe to estimate mixed-isospin corrections from other exclusive modes using the $\sim$1% estimate for each mode and adding these linearly. The mixed-isospin EM + SIB correction is thus under control, without need of lattice disconnected input (EM or otherwise), up to the $\sim 0.4 \times 10^{-10}$ uncertainty for non $2\pi, 3\pi$ exclusive-mode contributions. Second, the general analysis of the EM corrections to the $ab = 33$ and 88 parts of $a_\mu^{\mathrm{LO,HVP}}$ shows that these involve very strong cancellations. From the general forms, written in terms of the $SU(3)_F$-breaking loop factor ratios, it is clear these strong cancellations are entirely generic. Thus, unless the EM corrections to these quantities are much larger than the scale of the BMW results, we can be sure that these corrections are small without needing to know the precise values of the valence-valence disconnected EM contribution or the unsuppressed sea-sea connected contribution from the graph $D1$. Although some disconnected EM lattice results were used in the discussion above, the only substantive role these play is to confirm that the EM disconnected contributions do not have a massive enhancement relative to the expected "natural" $\sim$1% EM IB scale.

To conclude, we return to the reliability of treating the inclusive region [above $s = (1.937\ \mathrm{GeV})^2$ for KNT2019, above $s = (1.8\ \mathrm{GeV})^2$ for DHMZ] using pQCD. To be specific, we focus our discussion on the KNT2019 case. Uncertainties due to truncation in order and the uncertainty in the input α_s used are tiny, as are perturbative $D = 2$ corrections (the latter for the reasons outlined in Sec. IV E). The main uncertainty associated with the use of pQCD for the contribution from this region will thus most likely be that due to residual DV corrections. Let us consider the ansatz for the EM DVs used in the determination of α_s from electroproduction cross-section data detailed in Ref. [59]. This has the form

$$\rho^{\rm DV}_{\rm EM}(s) = \frac{5}{9}\rho^{\rm DV}_{ud;V}(s) + \frac{1}{9}\rho^{\rm DV}_{0,V}(s), \tag{7.1}$$

where $\rho^{\rm DV}_{ud;V}(s)$ is taken to have the large-s form

$$\rho^{\rm DV}_{ud;V}(s) = \exp\left(-\delta_1 - \gamma_1 s\right)\sin\left(\alpha_1 + \beta_1 s\right) \tag{7.2}$$

characterized by the DV parameters δ_1, γ_1, α_1, and β_1, which follows for massless quarks from the large-N_c and Regge arguments discussed in Ref. [48]. These DV parameters can be obtained from FESR fits to weighted integrals of the $I = 1$ vector-current spectral distributions measured in nonstrange hadronic τ decays. The τ-based results and their covariances were used as priors in the EM fits in Ref. [59]. The strange-quark contribution $\rho^{\rm DV}_{0,V}(s)$ was taken to have the same functional form, though with generally different DV parameters, reflecting the shift of resonances with hidden strangeness to higher locations in the spectrum. Reference [48] took $\gamma_0 = \gamma_1$ and $\beta_0 = \beta_1$ and fitted α_0 and δ_0 as free parameters, simultaneously refitting δ_1, γ_1, α_1, and β_1, subject to the input τ-based prior constraints. Let us rewrite the ansatz (7.1) in an alternate form with the $I = 0$ and 1 contributions explicitly separated:

$$\rho^{\rm DV}_{\rm EM}(s) = \frac{1}{2}\rho^{\rm DV}_{ud;V}(s) + \left[\frac{1}{18}\rho^{\rm DV}_{ud;V}(s) + \frac{1}{9}\rho^{\rm DV}_{0,V}(s)\right]. \tag{7.3}$$

The term in the square brackets is the $I = 0$ contribution. In this form, it is obvious that the DV ansatz of Ref. [59] produces a DV contribution to the $\rho^{\rm sconn+disc}_{\rm EM}(s)$ combination in which the light-quark part exactly cancels, leaving

$$\rho^{\rm sconn+disc;DV}_{\rm EM}(s) = \frac{1}{9}\rho^{\rm DV}_{0,V}(s). \tag{7.4}$$

In view of the significant recent improvement in the FESR analysis of the $I = 1$ vector channel reported in Ref. [60], we have updated the EM fits of Ref. [59] using as new light-quark DV priors the improved versions obtained in the fits of Ref. [60]. Using a range of different choices for the τ and EM FESR fit windows, we find integrated DV contributions to $a_\mu^{\rm LO,HVP}$ from the region above $s = (1.937\ {\rm GeV})^2$ lying in a narrow range around -0.25×10^{-10}. In view of the fact that the functional form for the DV ansatz in Eq. (7.2) was derived only in the massless limit but has also been employed for the strange-quark contribution, we treat this result as providing only a rough estimate of the uncertainty associated with neglecting possible residual integrated DV contributions in the region above $s = (1.937\ {\rm GeV})^2$. Even if one were to double this estimate, however, the resulting $\sim 0.5 \times 10^{-10}$ DV-induced uncertainty would still be small on the scale of the $\sim 1.5 \times 10^{-10}$ uncertainty of the strange-quark-connected plus disconnected and disconnected results obtained above.

ACKNOWLEDGMENTS

We thank Vladimir Druzhinin of *BABAR* for providing the $\rho \to 3\pi$ IB interference contribution portion of the 3π contribution to $a_\mu^{\rm LO,HVP}$ corresponding to the fit to $e^+e^- \to 3\pi$ cross section described in Ref. [56]; Gilberto Colangelo, Martin Hoferichter, and Peter Stoffer for providing the results of the zero-phase and free-phase dispersive fit determinations of the mixed-isospin IB 2π exclusive-mode contribution from the ρ-ω interference region; and Alex Keshavarzi for providing details of the combined KNT2019 exclusive-mode cross-section results used in the analysis above. D. B. is supported by São Paulo Research Foundation (FAPESP) Grant No. 2021/06756-6, by CNPq Grant No. 309847/2018-4, and by Coordenação de Aperfeiçoamento de Pessoal de Nível Superior—Brasil (CAPES)—Finance Code 001. M. G. is supported by the U.S. Department of Energy, Office of Science, Office of High Energy Physics, under Award No. DE-SC0013682. K. M. is supported by a grant from the Natural Sciences and Engineering Research Council of Canada. S. P. is supported by the Spanish Ministry of Science, Innovation and Universities (Project No. PID2020–112965 GB-I00/AEI/10.13039/501100011033) and by Grant No. 2017 SGR 1069. IFAE is partially funded by the CERCA program of the Generalitat de Catalunya. D. B. acknowledges the hospitality of the University of Vienna.

APPENDIX: REMAINING CHANNELS

The maximally conservative assessments for the remaining G-parity-ambiguous exclusive-mode contributions from the KNT2019 list are as follows:

(a) $K\bar{K}2\pi$: KNT2019 gives an $I = 0 + 1$ total of $[a_\mu^{\rm LO,HVP}]_{K\bar{K}2\pi} = 1.93(8) \times 10^{-10}$. Part of this contribution comes from the G-parity-negative $I = 0$ mode $\phi\pi\pi$. The *BABAR* $e^+e^- \to \phi\pi\pi$ cross-section results [58] (which were obtained by dividing the observed ϕ-region $K^+K^-\pi^+\pi^-$ cross sections by the then-current 2010 PDG $\phi \to K^+K^-$ branching fraction) produce a corresponding $I = 0$ all-ϕ-decay-mode $\phi\pi\pi$ contribution to $a_\mu^{\rm LO,HVP}$ of $0.192(12) \times 10^{-10}$. The $\phi(\to 3\pi)\pi\pi$ part of this contribution is already included in the listed 5π contributions. We have updated the *BABAR*-based all-ϕ-decay-mode result quoted above using the current PDG result for the $\phi \to K^+K^-$ branching fraction [34]. Multiplying this result by the current PDG two-mode $\phi \to K\bar{K}$ branching fraction sum, one finds the result $0.159(10) \times 10^{-10}$ for the $I = 0$, $\phi(\to K\bar{K})\pi\pi$ contribution to $[a_\mu^{\rm LO,HVP}]_{K\bar{K}2\pi}$. Subtracting this from the total $K\bar{K}2\pi$ contribution leaves a residual G-parity-ambiguous $K\bar{K}2\pi$ contribution of

$1.77(8) \times 10^{-10}$. Combining the small $I = 0$, $\phi(\to K\bar{K})\pi\pi$ contribution with the generic maximally conservative treatment of the latter then gives a strange-quark-connected plus disconnected contribution of

$$[a_\mu^{\text{sconn+disc}}]_{K\bar{K}2\pi} = 0.95(98) \times 10^{-10}. \quad \text{(A1)}$$

(b) $K\bar{K}3\pi$: KNT2019 gives an $I = 0 + 1$ total of $[a_\mu^{\text{LO,HVP}}]_{K\bar{K}3\pi} = 0.04(2) \times 10^{-10}$. The generic maximally conservative bound treatment thus gives a strange-quark-connected plus disconnected contribution of

$$[a_\mu^{\text{sconn+disc}}]_{K\bar{K}3\pi} = 0.02(2) \times 10^{-10}. \quad \text{(A2)}$$

(c) $X_1 = \omega(\to npp)K\bar{K}$ and $X_2 = \eta(\to npp)K\bar{K}$ (no ϕ): KNT2019 gives $I = 0 + 1$ totals of $[a_\mu^{\text{LO,HVP}}]_{X_1} = 0.00(0) \times 10^{-10}$ and $[a_\mu^{\text{LO,HVP}}]_{X_2} = 0.01(1) \times 10^{-10}$ for these two modes. The generic maximally conservative bound treatment thus gives a strange-quark-connected plus disconnected contribution of

$$[a_\mu^{\text{sconn+disc}}]_{X_1+X_2} = 0.00(1) \times 10^{-10} \quad \text{(A3)}$$

for the sum of the contributions from these two modes.

(d) $p\bar{p}$ and $n\bar{n}$: KNT2019 gives $I = 0 + 1$ totals of $[a_\mu^{\text{LO,HVP}}]_{p\bar{p}} = 0.03(0) \times 10^{-10}$ and $[a_\mu^{\text{LO,HVP}}]_{n\bar{n}} = 0.03(1) \times 10^{-10}$ for these two modes. The generic maximally conservative bound treatment thus gives a strange-quark-connected plus disconnected contribution of

$$[a_\mu^{\text{sconn+disc}}]_{p\bar{p}+n\bar{n}} = 0.03(3) \times 10^{-10} \quad \text{(A4)}$$

for the sum of the contributions from these two modes.

(e) Low-s $\pi^0\gamma$ and $\eta\gamma$: The $\pi^0\gamma$ and $\eta\gamma$ contributions from the higher-s region are strongly dominated by contributions from the large ω and ϕ peaks in the experimental cross sections, and hence are identifiable as $I = 0$. Such an $I = 0$ assignment is, however, less certain at low s, and we thus use the maximally conservative treatment in this region. With KNT2019 giving low-s $I = 0 + 1$ totals of $0.12(1) \times 10^{-10}$ and $0.00(0) \times 10^{-10}$ for these modes, this leads to a strange-quark-connected plus disconnected contribution of

$$[a_\mu^{\text{sconn+disc}}]_{\text{low-}s\pi^0\gamma+\eta\gamma} = 0.05(7) \times 10^{-10} \quad \text{(A5)}$$

for the sum of the contributions from these two modes.

[1] G. W. Bennett, B. Bousquet, H. N. Brown, G. Bunce, R. M. Carey, P. Cushman *et al.*, Phys. Rev. D **73**, 072003 (2006).
[2] B. Abi, T. Albahri, S. Al-Kilani, D. Allspach, L. P. Alonzi, A. Anastasi *et al.*, Phys. Rev. Lett. **126**, 141801 (2021).
[3] B. Chakraborty, C. T. H. Davies, G. C. Donald, R. J. Dowdall, J. Koponen, G. P. Lepage, and T. Teubner, Phys. Rev. D **89**, 114501 (2014).
[4] T. Blum, P. A. Boyle, T. Izubuchi, L. Jin, A. Jüttner, C. Lehner, K. Maltman, M. Marinkovic, A. Portelli, and M. Spraggs, Phys. Rev. Lett. **116**, 232002 (2016).
[5] B. Chakraborty, C. T. H. Davies, P. G. Oliviera, J. Koponen, G. P. Lepage, and R. S. VandeWater, Phys. Rev. D **96**, 034516 (2017).
[6] T. Blum, P. A. Boyle, L. Del Debbio, R. J. Hudspith, T. Izubuchi, A. Jüttner *et al.*, J. High Energy Phys. 04 (2016) 063; 05 (2017) 034(E).
[7] D. Giusti, V. Lubicz, G. Martinelli, F. Sanfilippo, and S. Simula, EPJ Web Conf. **175**, 06002 (2018).
[8] B. Chakraborty, C. T. H. Davies, C. De Tar, A. X. El-Khadra, E. Gamiz, S. Gottlieb *et al.*, Phys. Rev. Lett. **120**, 152001 (2018).
[9] Sz. Borsanyi, Z. Fodor, C. Hoelbling, T. Kawanai, S. Krieg, L. Lellouch *et al.*, Phys. Rev. Lett. **121**, 022002 (2018).
[10] D. Giusti, V. Lubicz, G. Martinelli, F. Sanfilippo, and S. Simula, J. High Energy Phys. 10 (2017) 157.
[11] T. Blum, P. A. Boyle, V. Gülpers, T. Izubuchi, L. Jin, C. Jung, A. Jüttner, C. Lehner, A. Portelli, and J. T. Tsang, Phys. Rev. Lett. **121**, 022003 (2018).
[12] D. Giusti, F. Sanfilippo, and S. Simula, Phys. Rev. D **98**, 114504 (2018).
[13] D. Giusti, V. Lubicz, G. Martinelli, F. Sanfilippo, S. Simula, and C. Tarantino, Proc. Sci. LATTICE2018 (**2018**) 140 [arXiv:1810.05880].
[14] V. Gülpers, A. Jüttner, C. Lehner, and A. Portelli, Proc. Sci. LATTICE2018 (**2018**) 134 [arXiv:1812.09562].
[15] D. Giusti, V. Lubicz, G. Martinelli, F. Sanfilippo, and S. Simula, Phys. Rev. D **99**, 114502 (2019).
[16] E. Shintani and Y. Kuramashi, Phys. Rev. D **100**, 034517 (2019).
[17] C. T. H. Davies, C. De Tar, A. X. El-Khadra, E. Gamiz, S. Gottlieb, D. Hatton *et al.*, Phys. Rev. D **101**, 034512 (2020).
[18] A. Gérardin, M. Cè, G. von Hippel, B. Hörz, H. B. Meyer, D. Mohler, K. Ottnad, J. Wilhelm, and H. Wittig, Phys. Rev. D **100**, 014510 (2019).
[19] C. Aubin, T. Blum, C. Tu, M. Golterman, C. Jung, and S. Peris, Phys. Rev. D **101**, 014503 (2020).

[20] Sz. Borsanyi, Z. Fodor, N. Guenther, C. Hoelbling, S. D. Katz, L. Lellouch *et al.*, Nature (London) **593**, 51 (2021).
[21] C. Lehner and A. S. Meyer, Phys. Rev. D **101**, 074515 (2020).
[22] C. Aubin, T. Blum, M. Golterman, and S. Peris, arXiv: 2110.03408.
[23] D. Giusti and S. Simula, arXiv:2111.15329.
[24] A. Risch and H. Wittig, arXiv:2112.00878.
[25] J. P. Lees, V. Poireau, V. Tisserand, E. Grauges, A. Palano, G. Eigen *et al.* (*BABAR* Collaboration), Phys. Rev. D **98**, 032010 (2018).
[26] A. Keshavarzi, D. Nomura, and T. Teubner, Phys. Rev. D **97**, 114025 (2018).
[27] A. Keshavarzi, D. Nomura, and T. Teubner, Phys. Rev. D **101**, 014029 (2020).
[28] M. Davier, A. Höcker, B. Malaescu, and Z. Zhang, Eur. Phys. J. C **80**, 241 (2020); **80**, 410(E) (2020).
[29] T. Aoyama, N. Asmussen, M. Benayoun, J. Bijnens, T. Blum *et al.*, Phys. Rep. **887**, 1 (2020).
[30] B. E. Lautrup, A. Peterman, and E. de Rafael, Phys. Rep. **3**, 193 (1972).
[31] E. de Rafael, Phys. Lett. B **322**, 239 (1994).
[32] T. Blum, Phys. Rev. Lett. **91**, 052001 (2003).
[33] D. Bernecker and H. B. Meyer, Eur. Phys. J. A **47**, 148 (2011).
[34] P. A. Zyla *et al.* (Particle Data Group), Prog. Theor. Exp. Phys., **2020**, 083C01 (2020).
[35] J. Z. Bai, Y. Ban, J. G. Bian, A. D. Chen, H. F. Chen, H. S. Chen *et al.* (BES Collaboration), Phys. Rev. Lett. **88**, 101802 (2002).
[36] M. Ablikim, J. Z. Bai, Y. Bai, Y. Ban, X. Cai, H. F. Chen *et al.* (BES Collaboration), Phys. Lett. B **677**, 239 (2009).
[37] V. V. Anashin, O. V. Anchugov, V. M. Aulchenko, E. M. Baldin, G. N. Baranov, A. K. Barladyan *et al.* (KEDR Collaboration), Phys. Lett. B **788**, 42 (2019).
[38] Y.-S. Tsai, Phys. Rev. D **4**, 2821 (1971); **13**, 771(E) (1976).
[39] Y. Amhis, Sw. Banerjee, E. Ben-Haim, F. U. Bernlochner, M. Bona, A. Bozek *et al.* (HFLAV Collaboration), Eur. Phys. J. C **81**, 226 (2021).
[40] B. Aubert, M. Bona, D. Boutigny, Y. Karyotakis, J. P. Lees, V. Poireau *et al.* (*BABAR* Collaboration), Phys. Rev. D **77**, 092002 (2008).
[41] M. Davier, S. Descotes-Genon, A. Hocker, B. Malaescu, and Z. Zhang, Eur. Phys. J. C **56**, 305 (2008).
[42] P. A. Baikov, K. G. Chetyrkin, and J. H. Kuhn, Phys. Rev. Lett. **101**, 012002 (2008).
[43] M. Beneke and M. Jamin, J. High Energy Phys. 09 (2008) 044.
[44] D. Boito, P. Masjuan, and F. Oliani, J. High Energy Phys. 08 (2018) 075.
[45] I. Caprini, Phys. Rev. D **100**, 056019 (2019).
[46] M. Jamin, Eur. Phys. J. Special Topics **230**, 2609 (2021).
[47] K. G. Chetyrkin and A. Kwiatkowski, Z. Phys. C **59**, 525 (1993).
[48] D. Boito, I. Caprini, M. Golterman, K. Maltman, and S. Peris, Phys. Rev. D **97**, 054007 (2018).
[49] J. Gasser, A. Rusetsky, and I. Scimemi, Eur. Phys. J. C **32**, 97 (2003).
[50] S. Aoki, Y. Aoki, D. Becirevic, T. Blum, G. Colangelo, S. Collins *et al.*, Eur. Phys. J. C **80**, 113 (2020).
[51] C. L. James, R. Lewis, and K. Maltman, Phys. Rev. D **105**, 053010 (2022).
[52] G. Colangelo, M. Hoferichter, and P. Stoffer, J. High Energy Phys. 02 (2019) 006.
[53] See, e.g., Martin Hoferichter's slides in the rho_omega_ phase.pdf from the Tuesday, June 29, afternoon discussion session of the 2021 KEK Muon $g-2$ Theory Initiative Workshop.
[54] G. Colangelo, M. Hoferichter, and P. Stoffer (private communication).
[55] C. E. Wolfe and K. Maltman, Phys. Rev. D **80**, 114024 (2009).
[56] J. P. Lees, V. Poireau, V. Tisserand, E. Grauges, A. Palano, G. Eigen *et al.* (*BABAR* Collaboration), Phys. Rev. D **104**, 112003 (2021).
[57] V. Druzhinin (private communication).
[58] J. P. Lees, V. Poireau, E. Prencipe, V. Tisserand, J. Garra Tico, E. Grauges *et al.* (*BABAR* Collaboration), Phys. Rev. D **86**, 012008 (2012).
[59] D. Boito, M. Golterman, A. Keshavarzi, K. Maltman, D. Nomura, S. Peris, and T. Teubner, Phys. Rev. D **98**, 074030 (2018).
[60] D. Boito, M. Golterman, K. Maltman, S. Peris, M. V. Rodrigues, and W. Schaaf, Phys. Rev. D **103**, 034028 (2021).